

# Simulations of single and two-component galaxy decompositions for spectroscopically selected galaxies from the Sloan Digital Sky Survey

Alan Meert,<sup>1\*</sup> Vinu Vikram,<sup>1†</sup> and Mariangela Bernardi<sup>1‡</sup>

<sup>1</sup>*Department of Physics and Astronomy, University of Pennsylvania, Philadelphia, PA 19104, USA*

Accepted 2013 May 7. Received 2013 April 29; in original form 2012 November 26

## ABSTRACT

We present the results of fitting simulations of an unbiased sample of SDSS galaxies utilizing the fitting routine GALFIT and analysis pipeline PyMorph. These simulations are used to test the two-dimensional decompositions of SDSS galaxies. The simulations show that single Sérsic models of SDSS data are recovered with  $\sigma_{\text{mag}} \approx 0.025$  mag and  $\sigma_{\text{radius}} \approx 5\%$ . The global values (half-light radius and magnitude) are equally well constrained when a two-component model is used. Sub-components of two-component models present more scatter. SDSS resolution is the primary source of error in the recovery of models. We use a simple statistical correction of the biases in fitted parameters, providing an example using the Sérsic index. Fitting a two-component Sérsic + Exponential model to a single Sérsic galaxy results in a noisier, but unbiased, recovery of the input parameters ( $\sigma_{\text{totalmag}} \approx 0.075$  mag and  $\sigma_{\text{radius}} \approx 10\%$ ); fitting a single Sérsic profile to a two-component system results in biases of total magnitude and half-light radius of  $\approx 0.05 - 0.10$  mag and 5%-10% in radius. Using an F-test to select the best fit model from among the single- and two-component models is sufficient to remove this bias. We recommend fitting a two-component model to all galaxies when attempting to measure global parameters such as total magnitude and half-light radius.

**Key words:** galaxies: structural parameters – galaxies: fundamental parameters – galaxies: catalogs – methods: numerical – galaxies: evolution

## 1 INTRODUCTION

Measurement of fundamental galaxy properties is an essential step in analyzing galaxy structure, formation, and evolution. At the most basic level, luminosity, size, and morphology are important properties, useful in evaluating dynamical and evolutionary models (e.g., Shankar et al. 2013). Non-parametric methods exist to estimate luminosity, size, and structure without imposing a functional form on a galaxy (e.g., Petrosian 1976; Abraham et al. 1996; Blanton et al. 2001). However, non-parametric methods are sensitive to the depth of the image and to the PSF. This can result in underestimating the luminosity and size of an object due to missing flux in faint regions of the galaxy or when the true size of the galaxy becomes small relative to the size of the angular PSF (Blanton et al. 2001, 2003).

Parametric methods offer a reasonable way to extrapolate galaxy light profiles into fainter regions at the expense of introducing a potentially incorrect functional form for the galaxy. Common functional forms used in parametric fitting include the  $r^{1/4}$  and the  $r^{1/n}$  models originally presented by de Vaucouleurs (1948) and Sérsic (1963). Empirical study suggests that bulges and elliptical galaxies are better described by de Vaucouleurs profiles or Sérsic profiles with Sérsic index  $n \approx 4$ . Disks and late-type spirals are best described by exponential profiles or Sérsic profiles with Sérsic index  $n \approx 1$  (Freeman 1970). More recent work has shown that the relationship between Sérsic index and the photometric or kinematic components of a galaxy is more complicated. Following Kent (1985), many studies simultaneously fit a second component in order to better accommodate the qualitative differences of bulges and disks in galaxies. Additionally, Caon, Capaccioli & D’Onofrio (1993) showed that the Sérsic profile is a better fit to many early-type galaxies than the traditional de Vaucouleurs profile.

\* E-mail: ameert@physics.upenn.edu

† E-mail: vvivuv@gmail.com

‡ E-mail: bernardm@sas.upenn.edu

There have been several catalogs of photometric galaxy decompositions presented recently (Simard et al. 2011; Kelvin et al. 2012; Lackner & Gunn 2012) with particular interest on the applicability of large sets of image decompositions to evolutionary models. However, systematic effects continue to be of concern, and the reliability of two-component decompositions in cases of low to moderate signal-to-noise are often viewed with some skepticism. In order to quantify the systematics and robustness of the  $\sim 7 \times 10^5$  fits of g, r, and i band SDSS spectroscopic galaxies to be presented in Meert, Vikram & Bernardi (2013), hereafter referred to as M2013, we generate simulations of single and two-component galaxies, referred to as “mocks,” and fit them using the same PyMorph pipeline (Vikram et al. 2010) used for the photometric decompositions presented in M2013. The M2013 catalog has already been used in Bernardi et al. (2013) to study systematics in the size-luminosity relation, in Shankar et al. (2013) to study size-evolution of spheroids, and in Huertas-Company et al. (2012) to study the environmental dependence of the mass-size relation of early-type galaxies.

Following several detailed studies which have used simulations to test the robustness of different fitting algorithms (e.g., Simard et al. 2002; Häußler et al. 2007; Lackner & Gunn 2012), the main goal of this paper is to test the robustness of PyMorph pipeline software on SDSS galaxies. We use these simulations to test the effects of increased signal-to-noise as well as increased resolution, PSF errors, and sky determination. Our simulations are specifically applicable to SDSS galaxies and are useful for evaluating the decompositions presented in M2013. We use unbiased samples to estimate and correct the systematic error on recovered parameters as well as estimate reasonable uncertainties on fit parameters.

A description of the simulation process is presented in Section 2. This includes constructing a catalog of realistic galaxy parameters (Section 2.1); generating galaxy surface brightness profiles based on these parameters (Section 2.2); generating sky and noise (Sections 2.3 and 2.4); and including seeing effects in the final image. The completed simulations are run through the fitting pipeline, and the fits are analyzed in Section 3. We examine the recovery of structural parameters in noise-free images (Section 3.1) and parameter recovery in realistic observing conditions including both neighboring sources and the effects of incorrect PSF estimation (Section 3.2). Recovery of mock galaxies is unbiased for single Sérsic models. However, two-component mocks are biased when fitted with single Sérsic profiles. This bias consists of an overestimate of the size and luminosity of the galaxy. PyMorph is further tested by inserting mocks into real SDSS images to test the dependence on local density (Section 3.3). We examine dependence of the fits on resolution and signal-to-noise (Section 3.4). The effect of changing the fitted cutout size (Section 3.5) and the effect of incorrect background estimation (Section 3.6) are also examined. In Section 4 we discuss the overall scatter in our fits and the implications of the simulations. Finally, in Section 5 we provide concluding remarks.

We generate single-component Sérsic galaxy models (hereafter referred to as **Ser**) and two forms of two-component galaxy models: one is a linear combination of de Vacouleurs and an exponential profile (**DevExp**) and

the other replaces the de Vacouleurs with a Sérsic profile (**SerExp**). A good overview of the Sérsic profile used throughout this paper is presented in Graham & Driver (2005). Throughout the paper, a  $\Lambda$ CDM cosmology is assumed with  $(h, \Omega_m, \Omega_\Lambda) = (0.7, 0.28, 0.72)$  when necessary.

## 2 CREATING THE SIMULATIONS

### 2.1 Selecting the simulation catalog

We create a set of mocks using fits from the photometric decompositions presented in M2013. These galaxy parameters represent the r-band image decompositions of a complete sample of the SDSS spectroscopic catalog containing all galaxies with spectroscopic information in SDSS DR7 (Abazajian et al. 2009).

The sample contains galaxies with extinction-corrected r-band Petrosian magnitudes between 14 and 17.77. The lower limit of 17.77 mag in the r-band is the lower limit for completeness of the SDSS Spectroscopic Survey (Strauss et al. 2002). The galaxies are also required to be identified by the SDSS **Photo** pipeline (Lupton et al. 2001) as a galaxy (**Type** = 3), and the spectrum must also be identified as a galaxy (**SpecClass** = 2). Additional cuts on the data following Shen et al. (2003) and Simard et al. (2011) are applied. Any galaxies with redshift  $< 0.005$  are removed to prevent redshift contamination by peculiar velocity. Galaxies with saturation, deblended as a PSF as indicated by the **Photo** flags, or not included in the Legacy survey<sup>1</sup> are also removed from the sample. In addition, following Strauss et al. (2002) and Simard et al. (2011), we apply a surface-brightness cut of  $\mu_{50, r} < 23.0$  mag/arcsec<sup>2</sup> because there is incomplete spectroscopic target selection beyond this threshold. After applying all data cuts, a sample of 670,722 galaxies remains. We select an unbiased sample of galaxies from the DR7 sample and use the fitted models from PyMorph to generate the mocks used in this paper.

For each model (**Ser**, **DevExp**, and **SerExp**), we select a representative sub-sample physically meaningful photometric decompositions. In order to ensure that the galaxies are representative of the full catalog, we examined the distributions of basic observational parameters of SDSS galaxies (surface brightness, redshift, apparent Petrosian magnitude, Petrosian half-light radius, and absolute magnitude).

Some restrictions on fit parameters are necessary to ensure that outliers are removed from the parameter space used to generate the simulations. Galaxies that do not satisfy these basic cuts are removed to ensure that the parameters used to generate the images are physically motivated. The cuts do not significantly bias our galaxy distribution as is shown in Figure 1. The cuts are:

- (i) Any Sérsic components must have Sérsic index less than 8.
- (ii) Half-light radius of any Sérsic component must be less than 40 kpc.
- (iii) In the two-component fits, the ratio of the bulge half-light radius to disk scale radius should be less than 1, or the galaxy should be bulge dominated ( $B/T > 0.5$ ).

<sup>1</sup> A list of fields in the Legacy survey is provided at <http://www.sdss.org/dr7/coverage/allrunsdr7db.par>

Conditions (i) and (ii) are used to prevent selection of **Ser** models with extended profiles that are likely the result of incorrect sky estimation during the fitting process. Condition (iii) ensures that any disk dominated galaxies have a bulge component that is smaller than the disk.

After enforcing the cuts on the sample, 10,000 fitted galaxy profiles for each of the **Ser**, **DevExp**, and **SerExp** models are selected at random without regard to the morphological classification of the original galaxy. The fitted parameters of these sample galaxies are used to generate the mocks used in testing the pipeline.

Selecting galaxy samples independent of galaxy morphology allows the **DevExp** and **SerExp** samples to contain some galaxies that do not truly possess a second component. Additionally, there will be some truly two-component galaxies (i. e., both bulge and disk components are present) that are misrepresented by a single Sérsic fit. However, this sampling method will not invalidate the results of our tests. Since we seek to test the ability to recover simulated galaxy parameters, we only require a realistic sample of galaxy profiles. Our samples satisfy this requirement. Single Sérsic galaxies in the original sample, simulated as mock **Ser** galaxies and fit with **Ser** models, test the ability to recover Sérsic parameters. Similarly, **Ser** mocks with **SerExp** models, show bias resulting from over-fitting a galaxy. Fitting the **SerExp** mocks with a **Ser** model shows the bias due to under-fitting.

Fitting a single-component model regardless of galaxy structure or morphology is a common practice (e.g., Blanton et al. 2005; Häussler et al. 2007; Simard et al. 2011). In Figure 8b we show that bias of 0.05 mags and 5% of the half-light radius result from fitting a two-component galaxy with a single component and that this bias increases to 0.1 mags and 10% of the half-light radius for brighter galaxies. These biases are important in analyzing the results of a single-component fitting catalog. For example, Bernardi et al. (2013) shows that intermediate B/T galaxies can often be fit by Sérsic models with large Sérsic indices, which can lead to misclassification if cuts similar to Shen et al. (2003) are used.

Figure 1 shows the distributions of surface brightness, redshift, extinction-corrected r-band Petrosian magnitude, r-band Petrosian half-light radius, and absolute magnitude of all SDSS spectroscopic galaxies (in black) and our simulation samples: **Ser** (red), **DevExp** (green), and **SerExp** (blue). The distribution of mock galaxies reproduces the observed distribution for all three samples for each observational parameter as verified by a KS 2-sample test.

Figure 1 also presents the signal-to-noise (S/N) of the mock samples as compared to the parent distribution. The S/N of the images is a limiting factor in the fitting process, so care must be taken to ensure that the S/N is not artificially increased in the simulations when compared to true SDSS galaxies. This S/N is calculated using the r-band Petrosian magnitude and r-band Petrosian half-light radius. Petrosian quantities are used to make a fairer comparison among all the samples. Because the Petrosian quantities are non-parametric, they avoid the complications that arise in assessing the possible biases introduced during fitting. Any differences in S/N are not large enough to significantly bias the distributions as verified by the KS 2-sample test. Therefore, we conclude that our samples are fair representations of

the underlying distribution of SDSS spectroscopic galaxies. The S/N is discussed further in Section 2.4.

Testing the accuracy of the PyMorph fitting routine does not necessarily require an unbiased parameter distribution. In reality, all that is required is a sample with sufficient coverage of the parameter space represented by the data. The simulations use smooth profiles, simplifications of the true galaxies that are observed in SDSS. Examination of the results of fitting these simplified models and comparison to fits of true observed galaxies can potentially yield useful information regarding galaxy structure. In Bernardi et al. (2013), the simulations are used together with the decompositions of the SDSS spectroscopic sample to characterize the scatter in the size-luminosity relation as well as examine possible biases. In order to make these comparisons, an unbiased sample is required. The distributions shown in Figure 1 show that the simulations are appropriate to use for this purpose.

## 2.2 Generating the images

We generate the two-dimensional normalized photon distributions from the one-dimensional Sérsic profiles and the one-dimensional exponential profiles of each bulge and disk component. Disk components are only simulated where required, as is the case for two-component fits. When multiple components are to be simulated, each component's normalized photon distribution is generated separately and combined prior to generating the simulated exposure.

Two-dimensional galaxy profiles are treated as azimuthally symmetric one-dimensional galaxy light profiles that are deformed according to an observed ellipticity. The galaxy profiles are generated using the structural parameters generated from photometric decompositions as described in the previous section. Single-component galaxy profiles and the bulges of two-component galaxies are generated according to the Sérsic profile

$$I(r) = I_e \exp \left( -b_n \left[ \left( \frac{r}{R_e} \right)^{\frac{1}{n}} - 1 \right] \right) \quad (1)$$

$$b_n = 1.9992n - 0.3271$$

where Sérsic index ( $n$ ), half-light radius ( $R_e$ ), and surface brightness at  $R_e$  ( $I_e$ ) are selected simultaneously from the catalog described in the previous section.

For the **DevExp** and **SerExp** cases, an exponential disk (Equation 1 with  $n = 1$ ) is added to the Sérsic component to model the disk component of the galaxies. The disk is modeled using a slightly modified version of Equation 1. This model requires input parameters scale radius ( $R_d$ ) and central surface brightness ( $I_d$ ).

$$I_{Exp}(r) = I_d \exp \left( \frac{-r}{R_d} \right). \quad (2)$$

After generating the two-dimensional profile, the image is pixelated by integrating over each pixel area. The details of this integration are largely unimportant. However, the simulation must take careful account of the integration in the central pixels, where the profile can vary greatly over a single pixel. Various oversampling methods have been devised to properly correct this common problem

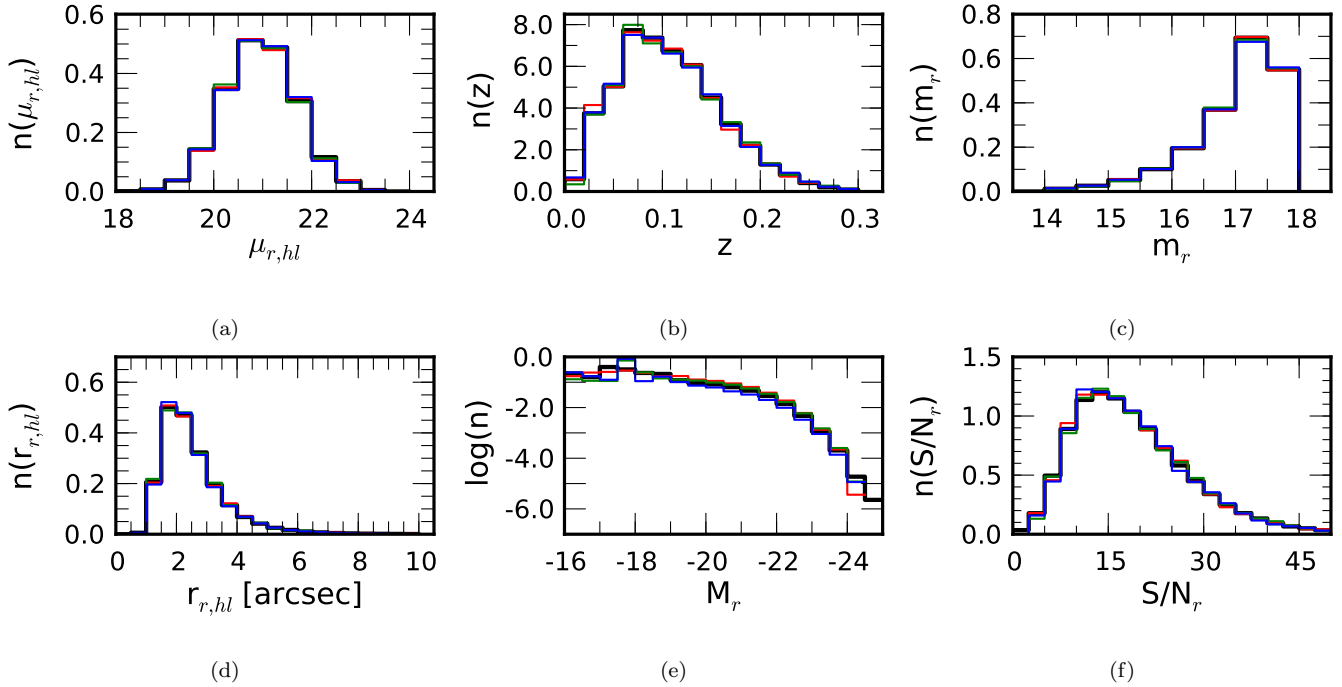


**Figure 1.** **a** The surface brightness distribution, **b** redshift distribution, **c** extinction-corrected r-band Petrosian magnitude, **d** r-band Petrosian halflight radius, **e**  $V_{\max}$ -weighted luminosity function, and **f** signal-to-noise distribution of the samples used in this paper drawn from the DR7 SDSS spectroscopic galaxy sample. The distribution of all SDSS spectroscopic galaxies is shown in black. Distributions of the *Ser*, *DevExp*, and *SerExp* mocks are shown in red, green, and blue, respectively. Bin counts are normalized to integrate to 1. The distributions of the mocks are representative of the full sample fitted in M2013 and are appropriate to compare to the SDSS spectroscopic sample as verified by a Kolmogorov-Smirnov 2-sample test. The signal-to-noise (S/N) will be discussed further in Section 2.4. In calculating this S/N, we use the measurement of sky provided by the PyMorph pipeline rather than SDSS to identify and separate target counts from sky counts. PyMorph sky estimation is shown to be more accurate than the SDSS estimation provided in the DR7 catalog.

(e.g., Peng et al. 2002; Häussler et al. 2007). The simulations in this paper have been tested to ensure that the pixel-by-pixel integration is accurate to  $\approx 3\%$  of the corresponding Poisson noise in a given pixel. Therefore, we treat the simulations as exact calculations of the galaxy photon distributions since any noise from the integration contributes only a small amount to the total noise budget.

The pixelated galaxy is numerically convolved with a PSF extracted from SDSS DR7 data using `read_PSF` program distributed by SDSS<sup>2</sup>. The choice of this PSF is discussed in Section 3.2.

### 2.3 Creating the background

Two hundred background images, each equal in size to an SDSS fpC image, are also simulated for testing purposes. These images contain constant background and a randomly selected field of galaxies taken from an SDSS fpC image. The SDSS catalog provides rudimentary photometric decompositions of each star and galaxy. Galaxies are fit with an exponential disk and a de Vacouleurs ( $n = 4$ ) bulge independently. The best fit is reported as a linear combination of the two fits using the `fracdev` parameter to express the ratio of the de Vacouleurs model to the total light in the galaxy.

For the simulated background used in this paper, each

galaxy is generated using the combined profile of the two fits. The de Vacouleurs bulge and exponential disk component are separately simulated according to the magnitude, radius, ellipticity, and position angle reported in SDSS. Each component is simulated using the method described in Section 2.2. The background galaxy is constructed by adding the two components using the `fracdev` parameter. The galaxy is then inserted into the fpC image. Any foreground stars are also simulated as point sources and inserted into the image.

For the background sky counts in the image, we use the mean sky of all SDSS observations as given in the SDSS `photoobj` table by the `sky_r` parameter. The distribution of the sky flux is plotted in Figure 2 in units of counts (or DN) per pixel per exposure. The median and mean values for a 54 second SDSS exposure are  $\approx 125$  and  $\approx 130$  counts per pixel, respectively. We use the mean value of 130 counts per pixel as the background in our simulations. This sky background is applied to the entire chip as a constant background; no gradient is simulated across the image. Background gradients should be approximately constant across a single galaxy. This assumption is verified by inserting the simulated galaxies into real SDSS fpC images near known clusters, where the sky contribution should be higher and gradients are more likely. In Section 3.3 we show that there is little change in the behavior of the fits in these types of environments.

Previous work has improved the measurements of sky background (see Blanton et al. 2011). However, these cor-

<sup>2</sup> `read_PSF` is part of the `readAtlasImages-v5.4.11` package available at [http://www.sdss.org/dr7/products/images/read\\_psf.html](http://www.sdss.org/dr7/products/images/read_psf.html)

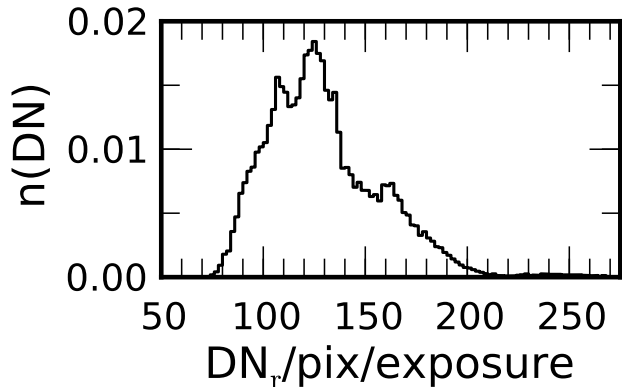


**Figure 2.** The distribution of sky values for data in the SDSS CASJOBS catalog. These data are drawn from the `sky_r` CASJOBS parameter and are converted into counts (DN) per pixel per standard SDSS image exposure of 54 seconds. We use this distribution to determine the sky value used in our simulations. As an approximation, we use the mean value of 130 counts/pixel/exposure.

rections tend to focus on areas of large, bright galaxies or on making the sky subtraction stable for purposes of tiling fpC images together. Since we are only focused on maintaining the proper S/N for our simulations, the sky levels provided in the SDSS database are sufficient, provided that they maintain the correct S/N. We discuss the S/N distribution of our simulations and the original SDSS galaxy sample in Section 2.4 below.

Diffraction spikes and other image artifacts are not directly simulated. However, the SDSS `photo` pipeline often misidentifies additional phantom sources along an observed diffraction spike. These phantom sources are modeled in our background, and so these effects are approximately modeled. It is reasonable to expect that the diffraction effects should not have a large effect on the fitting process, as their elongated straight structure does not mimic galaxy structure. The dominant effect produced by the bright stars in the field is bias in the background estimation in the nearby neighborhood of a star.

After simulation of the background images, and prior to adding noise, each background image is convolved with a random SDSS PSF selected from original fpC image upon which the individual image is based. Selecting PSFs from original SDSS images introduces a variation in PSF size between mock galaxies inserted into images and the background galaxies. However, this variation is not of concern for us in the fitting process because the vast majority of galaxies (over 90% of all galaxies) do not have neighbors near enough to the target galaxy to require simultaneous fitting. For these galaxies, the PSF applied to neighboring galaxies is of no interest in the fitting process because the sources are masked out. The details of this masking are not discussed in the remainder of the paper. Modifying the masking conditions produce no noticeable difference in the fitted values for our simulations. For the remaining 10% of galaxies, there may be some variation in the fit due to differing PSFs. PSF sizes can differ between target and neighboring galaxies by up to a factor of 2. However in practice, this happens for less than 1% of galaxies of the galaxies with neighbors. Furthermore, incorrect PSF tends to only cause effects at the centers

of galaxies. So although using a PSF that is different from the background PSF will affect the recovered parameters of the neighbor, it will not affect the target galaxy.

## 2.4 Noise

After generating a target galaxy and inserting it into a background, Poisson noise is added using the average inverse gain of an SDSS image ( $4.7 \text{ e}^-/\text{DN}$ ) and the average contribution of the dark current and read noise, referred to as the “dark variance,” ( $1.17 \text{ DN}^2$ ), to determine the standard deviation for each pixel. Specifically,

$$F_{i,j} \equiv I_{i,j} + \text{bkrd}_{i,j} \quad (3)$$

is the total flux in pixel  $(i, j)$  (i.e., the sum of the source and background fluxes in the pixel), and

$$\sigma_{i,j} = \sqrt{\frac{F_{i,j}}{\text{gain}} + \text{dark variance}} \quad (4)$$

so

$$\left(\frac{S}{N}\right)_{i,j} \equiv \frac{I_{i,j}}{\sigma_{i,j}}, \quad (5)$$

for a single pixel.

Since the fitting pipeline is dependent on the S/N, it is essential that the simulated S/N is comparable to SDSS. The distribution of the average S/N per pixel within the halfight radius for the simulations and the original galaxies is plotted in Figure 1f. The S/N distribution of simulations and the SDSS spectroscopic galaxies agree as verified by a KS 2-sample test, therefore the simulations appropriately approximate the S/N of SDSS galaxies contained in M2013.

An unbiased selection in the previously mentioned parameters is not sufficient to guarantee fair sampling of the S/N with respect to magnitude, nor does it prevent fictitious correlations among multiple fit parameters. In fact, correlations among fit parameters are to be expected if the PyMorph pipeline is robustly measuring properties of the target galaxies (many correlations exist among physical parameters). It is difficult, and largely unnecessary, to examine every possible relationship for correlations introduced by biases in the sample selection process.

Examining the S/N and the halfight radius versus apparent magnitude help to ensure the appropriateness of the simulation. Systematic differences in radius will lead to systematic variation in the S/N of the sample. We also examine the scatter in recovered fitting parameters as a function of magnitude. Therefore, the S/N as a function of apparent magnitude should appropriately reflect that of the parent sample from SDSS.

Figure 3 presents the halfight radius versus apparent magnitude, and Figure 4 presents the S/N versus apparent magnitude. The points shown in red and blue correspond to the `Ser` and `SerExp` mocks, respectively. The underlying SDSS parent distribution is shown in black. Figure 3 shows that the `Ser` and `SerExp` models are in close agreement with the full SDSS sample. The `Ser` and `SerExp` model radii agree across the magnitude range. The S/N agrees with the full SDSS sample or is slightly below that of SDSS. The lower signal-to-noise, although not exactly that of SDSS, will not bias the tests toward better results, so we deem these samples acceptable for testing. The `DevExp` sample, which is not

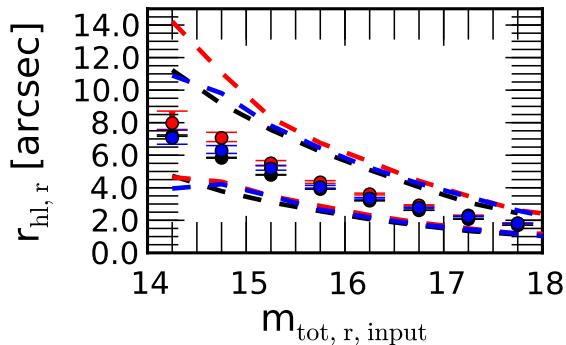


**Figure 3.** The distribution of galaxy radii as a function of apparent magnitude for the parent SDSS sample in black, the **Ser** model in red and the **SerExp** model in blue. The median in each bin is shown with error bars representing the 95% CI on the median. Corresponding dashed lines show the extent of the middle 68% of data. The **SerExp** model is in close agreement across the entire magnitude range while the **Ser** model begins to diverge at brighter magnitudes.

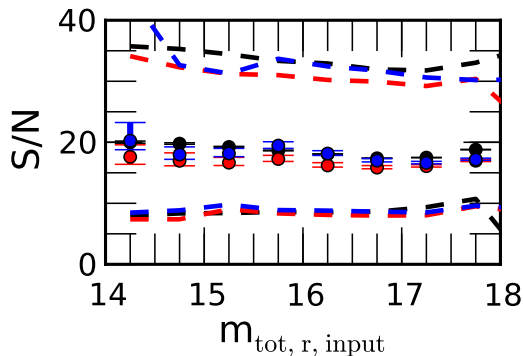


**Figure 4.** The distribution of galaxy S/N as a function of apparent magnitude is presented in the same format as Figure 3. The **SerExp** and **Ser** models are in close agreement with the full sample across the entire magnitude range.

shown here, tends to have smaller radii and higher S/N at brighter magnitude. The results of tests using the **DevExp** model are not discussed in the remainder of this paper. They can be found in M2013.

## 2.5 Final processing for fitting

For each mock galaxy, we also generate a weight image of the  $\sigma_{i,j}$  values according to Equation 4. This image is supplied along with the input image to the pipeline in order to calculate the  $\chi^2$  value for the fit.

Figure 5 shows some examples of mock galaxies throughout the simulation process. This includes the noiseless mock galaxy, the noiseless simulated background, the composite image of galaxy and background, and the composite image after adding Poisson noise with  $\sigma_{i,j}$  defined in Equation 4. The final image size used for fitting is 20 times the Petrosian r-band half-light radius. A discussion of this choice of stamp size is presented in Section 3.5.

## 3 TESTING PYMORPH IMAGE DECOMPOSITIONS

In order to test the parameter recovery of the PyMorph pipeline on SDSS spectroscopic galaxies, we apply the PyMorph pipeline to the mocks described in Section 2. The PyMorph pipeline uses GALFIT to fit smooth profiles to the mock galaxies. We apply the pipeline to several different realizations of our mock galaxies. These realizations increase in complexity from a noiseless image to an image with real noise and (possibly clustered) neighboring sources. We show that the ability of PyMorph to reliably recover model parameters is limited by both the S/N and the resolution of the mock galaxy. Understanding the systematic effects of S/N and resolution is useful in interpreting the data presented in M2013. It may also be used to correct biases in the data as described later in Section 4.

### 3.1 Noiseless images

As an initial test, the pipeline is applied to simulations prior to adding noise, background counts, or neighboring sources. This produces the minimum scatter in the data, serves to verify that our simulations are correct, and shows that PyMorph is properly functioning.

The total apparent magnitude, half-light radius, and additional fit parameters recovered by fitting the noiseless images of the **Ser** and **SerExp** models are presented in Figures 6a, 7a, 8a, 9a, and 10a. The plots show the difference in simulated and fitted values (fitted value - input value). The difference is shown versus the input magnitude as well as the input value of the respective fit parameter. The gray-scale shows the density of points in each plane with red points showing the median value. Error bars on the median value are the 95% confidence interval on the median obtained from bootstrapping. Blue dashed lines show the regions which contain 68% of the objects.

Figures 6a and 9a show the corresponding fit is well constrained (**Ser** fit with **Ser**, and **SerExp** with **SerExp**). The total magnitude and half-light radius are both constrained well within 1% error on the flux or radius ( $\sigma_{\text{total mag}} \approx 0.01$  mag and  $\sigma_{\text{radius}} \approx 1\%$ ). However, the scatter increases somewhat for the sub-components of the **SerExp** fit (see Figure 10a). As the components of the **SerExp** model become dim (bulge/disk magnitude approaches 18.5), the component contribution to the total light becomes small. The origin of the magnitude limit is merely an artifact of our selection criteria requiring that all galaxies have total magnitude brighter than 17.77. This implies that components with magnitude of  $\approx 18.5$  or dimmer are necessarily sub-dominant components and contribute at most  $\approx 50\%$  of the light to the total profile. On average, components dimmer than 18.5 magnitudes contribute about 25% of the total light to a typical galaxy in this sample, and this contribution drops rapidly to about 10% by 19 magnitudes. In these cases, the sub-dominant component will be much less apparent in the image and, therefore, less important to the overall  $\chi^2$  of the fit, allowing for greater error in the parameters of that component. In addition, once Poisson noise is considered, these dimmer components suffer from much lower S/N. Later tests (Section 3.4) show substantial error on these components due to the low flux and resulting low S/N.

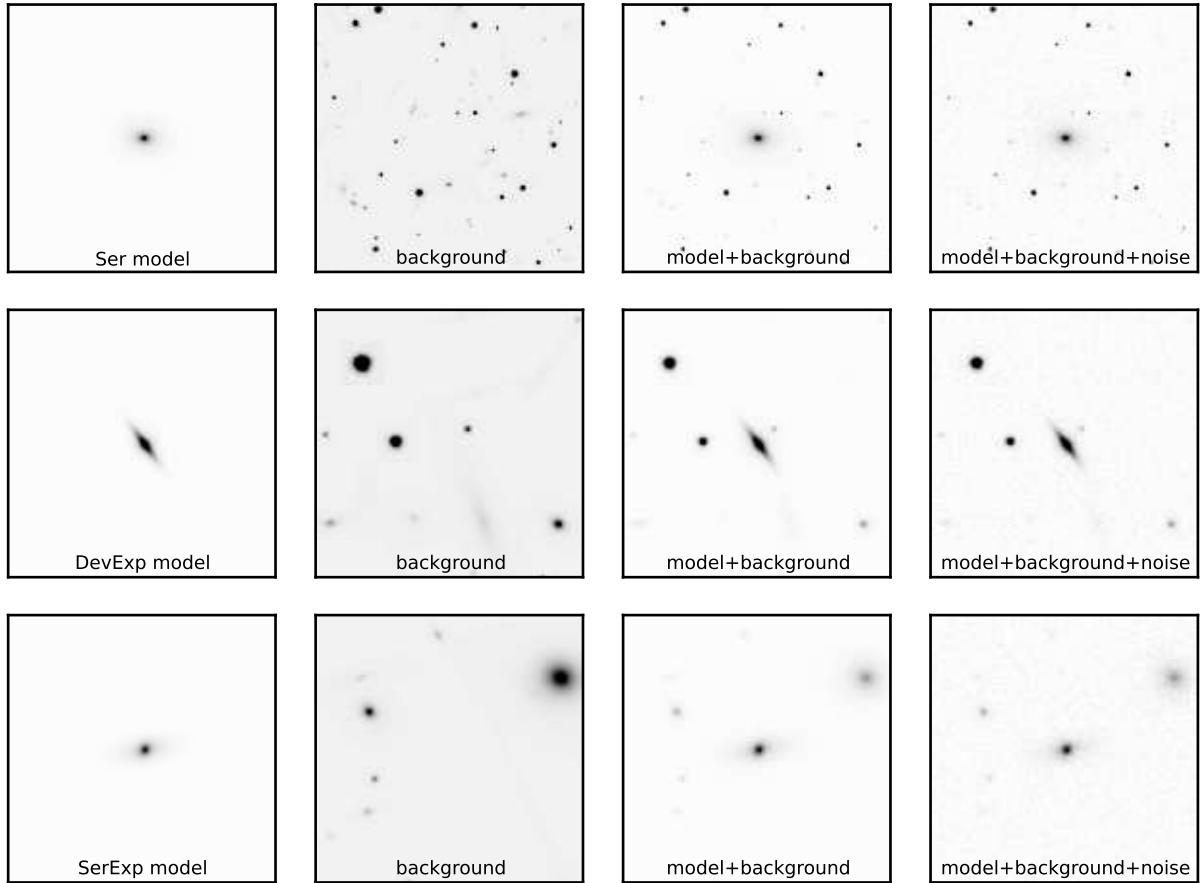


**Figure 5.** Examples of mock galaxies and background shown before and after adding Poisson noise. Top, middle, and bottom rows show randomly selected sample **Ser**, **DevExp**, and **SerExp** profiles, respectively. From left to right, the columns show the mock galaxy, simulated background, background+galaxy, and final image with noise.

Additionally, sub-dominant components (in particular, bulges) may be much smaller than the overall size of the galaxy. This makes bulge parameter recovery susceptible to resolution effects. These effects are also explored in Section 3.4.

The magnitude and halflight radius are also well constrained when a **Ser** galaxy is fit with a **SerExp** profile (Figure 7a). However, a **SerExp** galaxy fit with a **Ser** profile produces large biases in the magnitude and halflight radius (Figure 8a).

As already mentioned, the total magnitude and halflight radius are well constrained ( $\sigma_{\text{total mag}} \approx 0.01$  mag and  $\sigma_{\text{radius}} \approx 1\%$ ) in cases where the correct model is applied to the mocks (i.e., **Ser** mock fit with a **Ser** model). This is not always the case when the wrong model is applied (i.e., **SerExp** mock fit with a **Ser** model). When attempting to fit the simulated **SerExp** mocks with a **Ser** model, we find measurable bias of order .01 magnitudes in total magnitude. We also find the scatter of both the size and magnitude to be increased by an order of magnitude. This bias and increased scatter becomes even larger in later tests. It is obvious that a single-component galaxy cannot properly model a two-component galaxy in general, and therefore, we would expect significant problems in attempting to fit a

single-component profile to a two-component galaxy. Nevertheless, this type of fit is often performed on real data at low to moderate resolution and S/N where it is unlikely to recover a robust two-component fit. An important observation is that the **SerExp** fit provides the most stable estimate of the halflight radius and total magnitude regardless of the true simulated galaxy model (**Ser**, **DevExp**, or **SerExp**). The additional freedom in the **SerExp** model and the fact that the **Ser** and **DevExp** models are special cases of the **SerExp** model would lead us to expect this result. Therefore, it is advisable to always use a **SerExp** fit in the course of fitting SDSS galaxies unless there is specific evidence to the contrary.

One systematic effect in the pipeline that has been noted by other groups (e.g., Blanton et al. 2005; Guo et al. 2009), is the underestimate of Sérsic index at larger Sérsic indexes. At Sérsic indexes of  $n \approx 4$ , we underestimate the Sérsic index by less than 1%. However, this underestimate increases in the later tests. The data suggest that a substantial component of this error is due to the resolution limits of the SDSS sample. At larger Sérsic index, a high sampling rate at the center of the galaxy is useful in distinguishing the preferred value of the Sérsic index. We further explore the effect of image resolution in Section 3.4.

Since no Poisson noise is added to these images, the scatter apparent in these fits is a combination of the limitations of the SDSS data (in particular resolution), systematics inherent in the PyMorph routine (as well as the GALFIT routine used by PyMorph), and any parameter degeneracies inherent in the models.

GALFIT uses the Levenberg-Marquardt minimization method (Press et al. 1992) to find the minimum of the  $\chi^2$  distribution of the fit. The Levenberg-Marquardt method is not a global search algorithm but rather follows the steepest descent to a local minimum. As the parameter space becomes more complicated, GALFIT has more trouble accurately recovering parameters. Adding components to the fit (i. e., going from a one-component to two-component fit or going from a fixed Sérsic index component to one with a free Sérsic index) will not only complicate the  $\chi^2$  surface, making convergence less likely, but may introduce true degeneracies in the parameter space.

For instance, the **SerExp** fit of a galaxy of very late type often suffers from over-fitting. The bulge component will tend to fit the disk of the galaxy as a second disk component with  $n_{\text{bulge}} \approx 1$ . This is obviously an unintended solution to the fitting but one that is equally valid from an  $\chi^2$  perspective. In practice, it is difficult to prevent this type of convergence without artificially constraining the fitting routine. Such constraints are generally discouraged and can lead to other negative effects including convergence to a non-optimal solution. The best solution to the parameter degeneracy is close examination of any two-component fits in cases where  $n_{\text{bulge}} \approx 1$ , or B/T  $\approx 0$  or 1.

In addition, PyMorph reports statistical error estimates on the fitted parameters as returned from GALFIT. These errors are found to be an underestimate of the true error in the fits by as much as an order of magnitude. This gross underestimation of the error is also reported by Häussler et al. (2007) as well as being discussed in the GALFIT user notes<sup>3</sup>. Following Häussler et al. (2007), we examine the ratio of the uncertainty reported by GALFIT to the deviation of the measured parameters (referred to as  $\sigma/\Delta$ ).  $\sigma/\Delta$  should be greater than 1 for approximately 68% of the data if the estimated uncertainty is appropriate. However, this is not the case for any of the parameters in the fits. We discuss a simple method for correcting the systematic bias and estimating the uncertainty in Section 4.

### 3.2 The effects of background, neighbor sources, and incorrect PSF extraction

When analyzing real data, it is not possible to extract the PSF at the target galaxy to arbitrary accuracy. Interpolation is required and generally performed on a network of the nearest stars to the target galaxy. We test this effect through extraction of a neighboring PSF to be used during fitting in place of the PSF used to generate the image.

The neighbor PSF used in fitting is randomly selected from a location within a 200 pixel box surrounding the source. This provides approximately even sampling of distances from nearly 0 to about 170 pixels in separation from

the source which corresponds to a separation of  $\approx 0$  to  $\approx 67.32$  arcseconds between the target galaxy and the location used for PSF extraction. This inserts some PSF error into the process of fitting as would be expected in the case of real data. However, it also retains the similarity between the PSF used for simulation and the PSF used for fitting. A strong similarity between the two would be expected since the PSF generally will not vary greatly over the area of a single fpC image.

Target galaxies are randomly inserted into the simulated fpC images described in Section 2.3. The simulated fpC images contain sky as well as neighboring sources. The PSF of the neighboring sources will have a different PSF than the target galaxy. This effect is not of concern in this work.

Prior to fitting, a new cutout is extracted from the total image (containing the target galaxy and background) ensuring that the target galaxy is at the center of the stamp image. By constructing new postage stamp images in this manner, we ensure that there is sufficient variation in the background while preventing us from fitting the incorrect galaxy.

These fits (containing error in PSF reconstruction, neighboring sources, and noise) are the closest simulation to actual observing conditions that we have analyzed. Therefore the fits and the resulting measures of scatter and bias are adopted as our fiducial estimates of scatter and bias when using the pipeline.

Figures 6b, 7b, 8b, 9b, and 10b show that we recover the input values with marginal scatter. The total magnitude and halflight radius remain well constrained ( $\sigma_{\text{totalmag}} \approx 0.05$  mag and  $\sigma_{\text{radius}} \approx 5\%$ ) in cases where the correct model is fit to the mock galaxy. However, this scatter becomes larger when the wrong model is fit. The underestimate of the Sérsic index, particularly at large values, persists.

Further examination of the two-component fits show that the pipeline has difficulty extracting dim components (bulge or disk magnitude dimmer than  $\approx 18.5$ ). In these ranges, the components are observed at lower S/N and the pipeline loses sensitivity to the model parameters. The **SerExp** fit shows an underestimate of Sérsic index, which is even stronger than in the single-component case, and an underestimate of bulge radius. However, the disk parameters remain unbiased with an increase in scatter of the model parameters. The increased stability of the disk parameters relative to the bulge parameters was also noted in Simard et al. (2011). In their paper, the authors comment that this may be due to the fixed profile shape (due to the fixed Sérsic index,  $n = 1$ ) or to the fact that on average bulges are more compact than disks leading to a resolution effect. This stability is the result of the increased resolution as disk sizes in our sample are roughly 3 times the FWHM of the PSF while bulges are smaller, on average approximately equal to the FWHM of the PSF in size. We discuss this further in Section 3.4.

In general, the **SerExp** fits are problematic and require much care when analyzing individual components. However, as we have already shown, total magnitude and halflight radius are still tightly constrained.

Table 1 summarizes the bias and scatter in the fits; they exhibit trends with both the input value of the parameter and the input magnitude of the galaxy. This behavior is not

<sup>3</sup> See the technical FAQs at <http://users.obs.carnegiescience.edu/peng/work/galfit/TFAQ.htm>

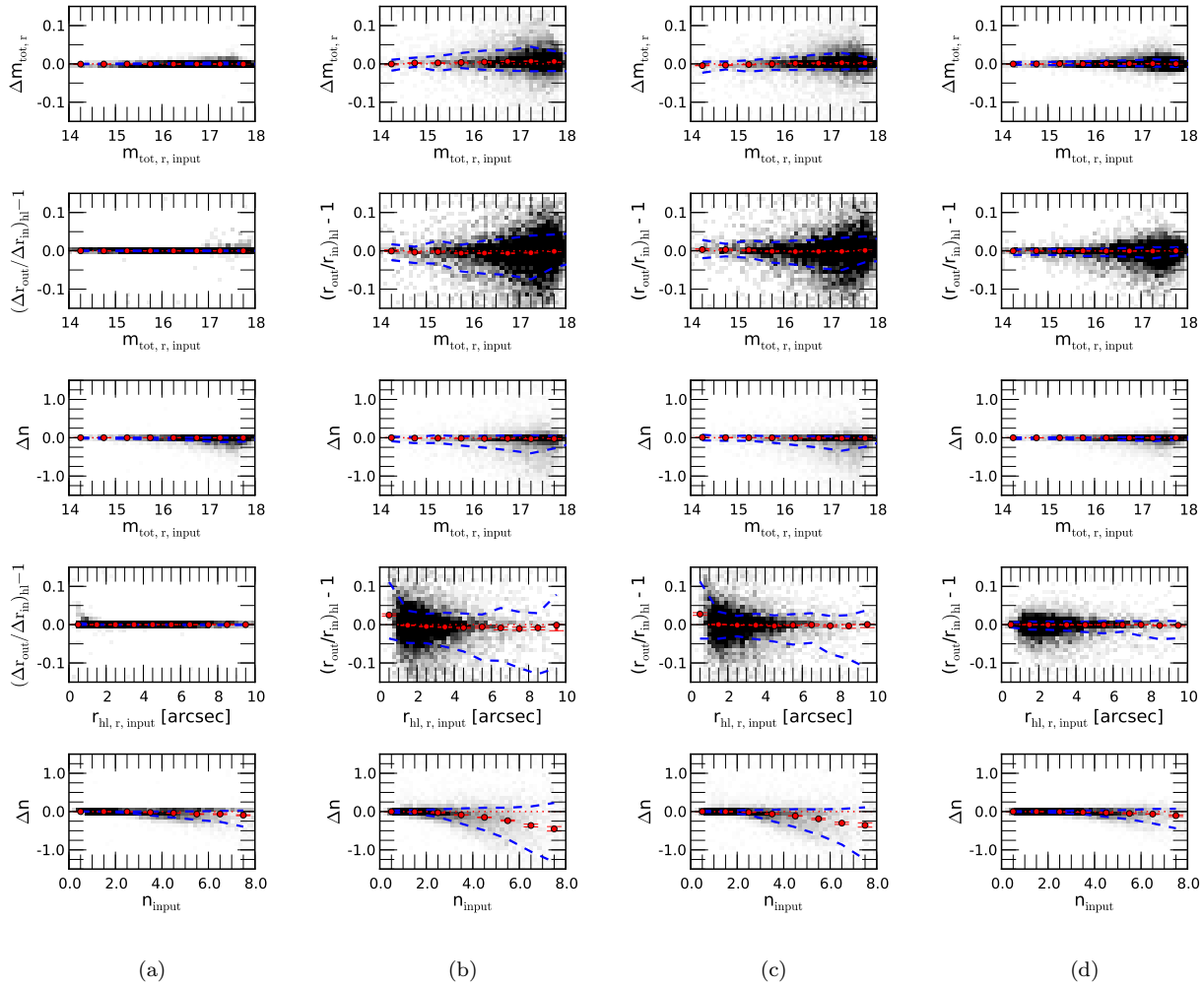


**Figure 6.** The simulated and recovered apparent magnitude, half-light radius, and Sérsic index for a **Ser** galaxy fit with a **Ser** model in four cases: **a** the image prior to adding Poisson noise, **b** our fiducial case with simulated sky, Poisson noise, PSF errors, and neighboring sources, **c** the fiducial case with S/N increased by a factor of 4, and **d** the fiducial case with resolution increased by a factor of 2. Over-plotted are the bias (red points) in the fitted values. All plots show the 68% (dashed line) scatter in blue. The density of points is plotted in gray-scale. The Sérsic index shows increasing underestimate up to  $\approx 0.5$  (or  $\approx 6\%$ ) at the largest Sérsic indexes.

properly encapsulated in the overall measure of bias, so these values are useful only as an example of the relative scale of bias and scatter for each parameter.

Errors can be correlated across many fit parameters, so we also calculate a correlation matrix for the parameter errors. Figure 11 shows an example of the correlation matrix for the **SerExp** mocks fit with a **SerExp** model. We see the expected strong correlations between bulge-to-light ratio and the bulge and disk magnitudes as well as the correlation among the radii of the bulge component with the Sérsic index. While the correlation matrix suggests that there is little correlation between sky estimation error and the fitted parameters, we will show later that there is indeed a strong correlation in model errors with sky estimation error.

The apparent lack of correlation of sky error with the other fitting parameters is somewhat surprising. However, Figures 14 and 15 suggest a possible explanation for the apparent lack of correlation. Correlation of parameter errors with sky errors is non-linear and asymmetric with respect to over- or underestimating the sky. The fits discussed in

this section are shown on Figures 14 and 15 in red. These points lie in a region where sky error does not significantly bias most parameters. In addition, the scatter of the sky values is quite small. This small scatter prevents us from sampling the broader covariance of the sky. If, for example, the recovered sky value was an underestimate of 0.5%, then there would be a measurable covariance of fitting parameters with sky due to the steepness of the parameter bias with respect to sky level. We discuss the sky estimation further in Section 3.6.

### 3.3 Testing with real images

To verify the validity of the simulated background and to test the fitting pipeline in clustered environments, we insert the mock galaxies into real SDSS fpC images. The fpC images are selected from SDSS DR7 images containing spectroscopic galaxy targets.

We omit plots of the fitted values here, because the scatter and the bias in the fits remain unchanged, sug-

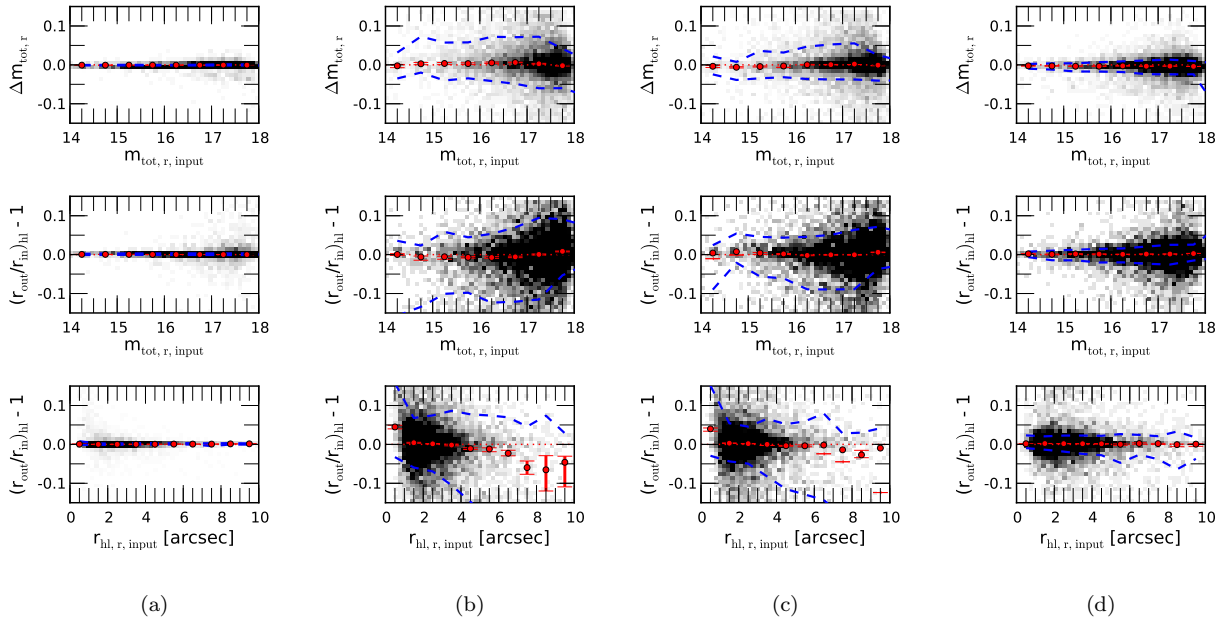


**Figure 7.** The simulated and recovered apparent magnitude and halfight radius for a *Ser* galaxy fit with a *SerExp* model in four cases: **a** the image prior to adding Poisson noise, **b** our fiducial case containing simulated sky, Poisson noise, PSF errors, and neighboring sources, **c** the fiducial case with S/N increased by a factor of 4, and **d** the fiducial case with resolution increased by a factor of 2. Over-plotted are the bias (red points) in the fitted values. All plots show the 68% (dashed line) scatter in blue. The density of points is plotted in gray-scale.

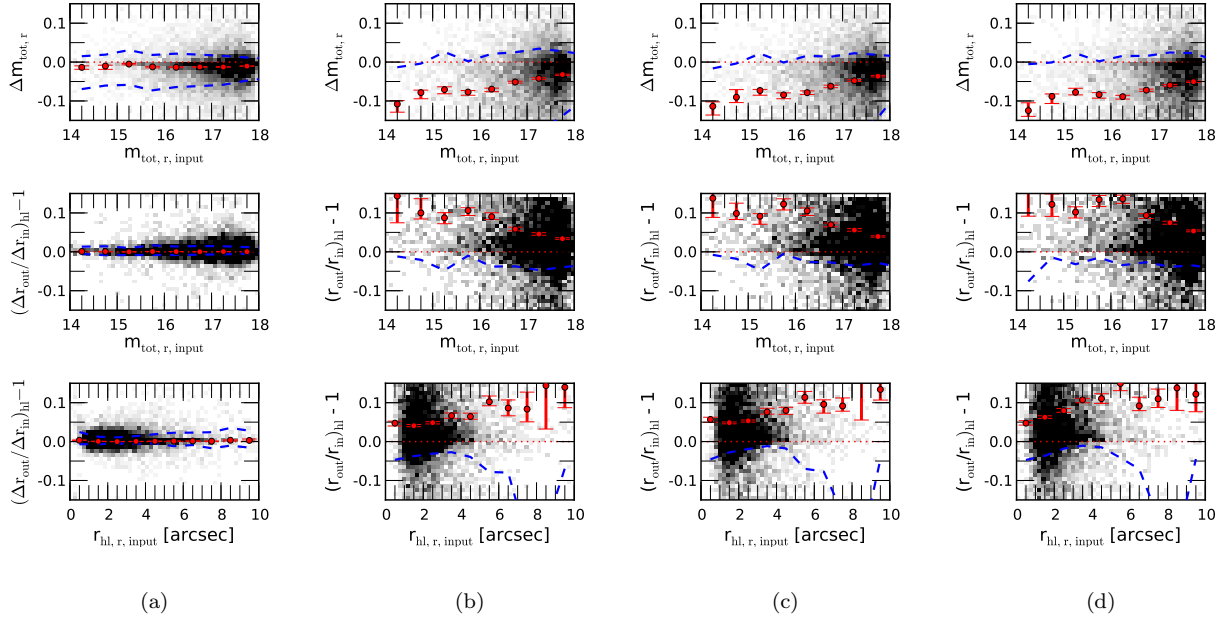


**Figure 8.** The simulated and recovered apparent magnitude and halfight radius for a *SerExp* galaxy fit with a *Ser* model in four cases: **a** the image prior to adding Poisson noise, **b** our fiducial case containing simulated sky, Poisson noise, PSF errors, and neighboring sources, **c** the fiducial case with S/N increased by a factor of 4, and **d** the fiducial case with resolution increased by a factor of 2. Over-plotted are the bias (red points) in the fitted values. All plots show the 68% (dashed line) scatter in blue. The density of points is plotted in gray-scale. The inability of the *Ser* profile to accurately model a *SerExp* galaxy is clearly evident. Errors in magnitude and halfight radius are correlated and the error in radius is largely driven by errors in the largest, brightest objects. However, systematic errors occur even at the dimmer magnitudes. *Ser* fits tend toward recovering larger, brighter objects when applied to a true two component galaxy.

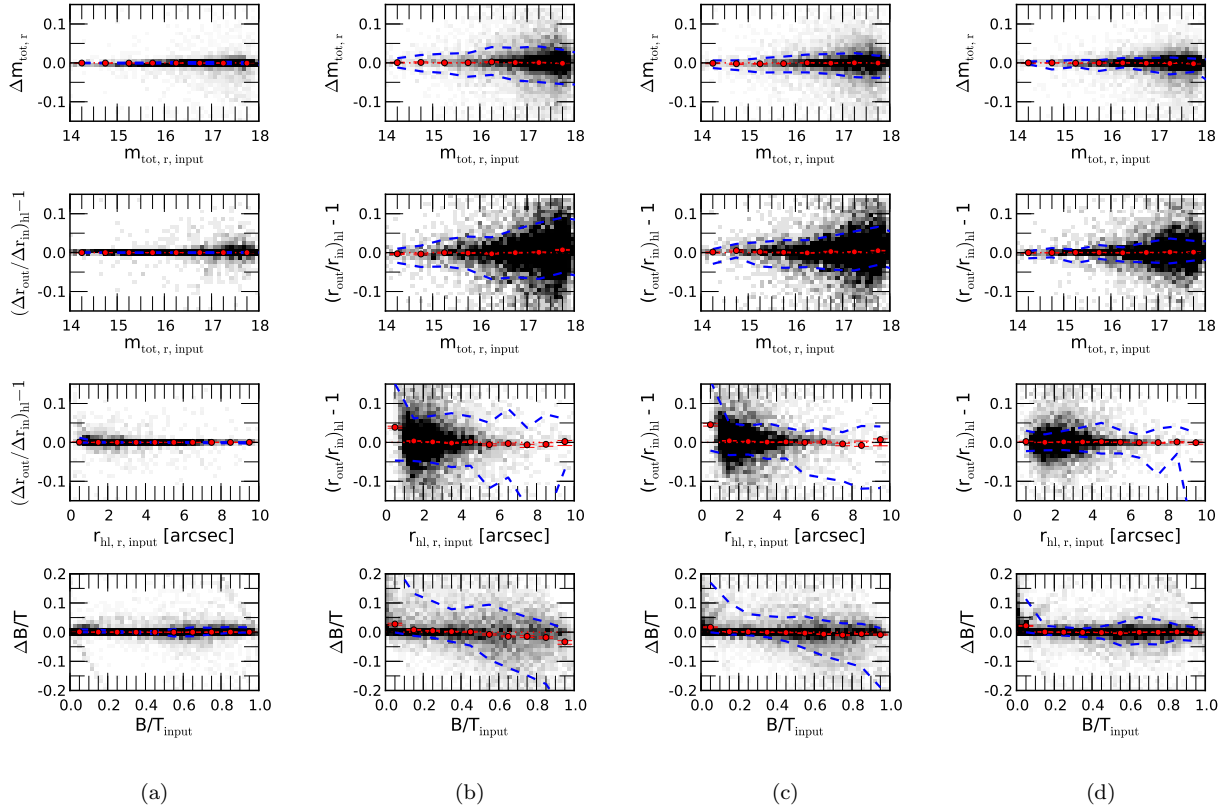


**Figure 9.** The simulated and recovered apparent magnitude, half-light radius, and bulge-to-total light ratio for a **SerExp** galaxy fit with a **SerExp** model in four cases: **a** the image prior to adding Poisson noise, **b** our fiducial case containing simulated sky, Poisson noise, PSF errors, and neighboring sources, **c** the fiducial case with S/N increased by a factor of 4, and **d** the fiducial case with resolution increased by a factor of 2. Over-plotted are the bias (red points) in the fitted values. All plots show the 68% (dashed line) scatter in blue. The density of points is plotted in gray-scale. The apparent trend in B/T from overestimation at lower B/T values to underestimation at higher B/T values is largely due to the boundaries on the parameter space forcing the scatter to be asymmetric (e. g., a galaxy with true B/T=1 cannot be estimated to have B/T>1).

Simulated model	Parameter	fitted model			
		Ser		SerExp	
		bias	1- $\sigma$	bias	1- $\sigma$
Ser	$m_{tot}$ [mag]	$0.00 \pm 0.09$	$[-0.02, 0.02]$	$-0.02 \pm 0.18$	$[-0.11, 0.02]$
	$r_{hl}$ [arcsec]	$-0.01 \pm 0.68$	$[-0.14, 0.01]$	$0.11 \pm 1.53$	$[-0.11, 0.04]$
	sky [%]	$-0.05 \pm 0.14$	$[-0.11, -0.05]$	$-0.05 \pm 0.14$	$[-0.11, -0.05]$
	Sérsic Index	$-0.08 \pm 0.57$	$[-0.44, 0.01]$	–	–
SerExp	$m_{tot}$ [mag]	$-0.07 \pm 0.18$	$[-0.22, -0.01]$	$-0.02 \pm 0.15$	$[-0.09, 0.01]$
	$r_{hl}$ [arcsec]	$0.49 \pm 1.86$	$[-0.02, 0.30]$	$0.07 \pm 1.17$	$[-0.07, 0.04]$
	sky [%]	$-0.08 \pm 0.15$	$[-0.16, -0.07]$	$-0.06 \pm 0.13$	$[-0.11, -0.05]$
	B/T	–	–	$0.00 \pm 0.15$	$[-0.07, 0.03]$
	$m_{bulge}$ [mag]	–	–	$-0.14 \pm 0.71$	$[-0.73, 0.06]$
	$m_{disk}$ [mag]	–	–	$-0.04 \pm 0.50$	$[-0.41, 0.05]$
	$r_{bulge}$ [arcsec]	–	–	$0.08 \pm 0.97$	$[-0.27, 0.11]$
	$r_{disk}$ [arcsec]	–	–	$0.07 \pm 0.82$	$[-0.14, 0.08]$
Sérsic Index	–	–	$0.06 \pm 1.98$	$[-0.90, 0.14]$	

**Table 1.** The bias and scatter of the fitted parameters of the simulated images with background and PSF effects. These values are provided for illustrative purposes only. There is much underlying structure in the errors when compared to their respective input values or the magnitude of the component.

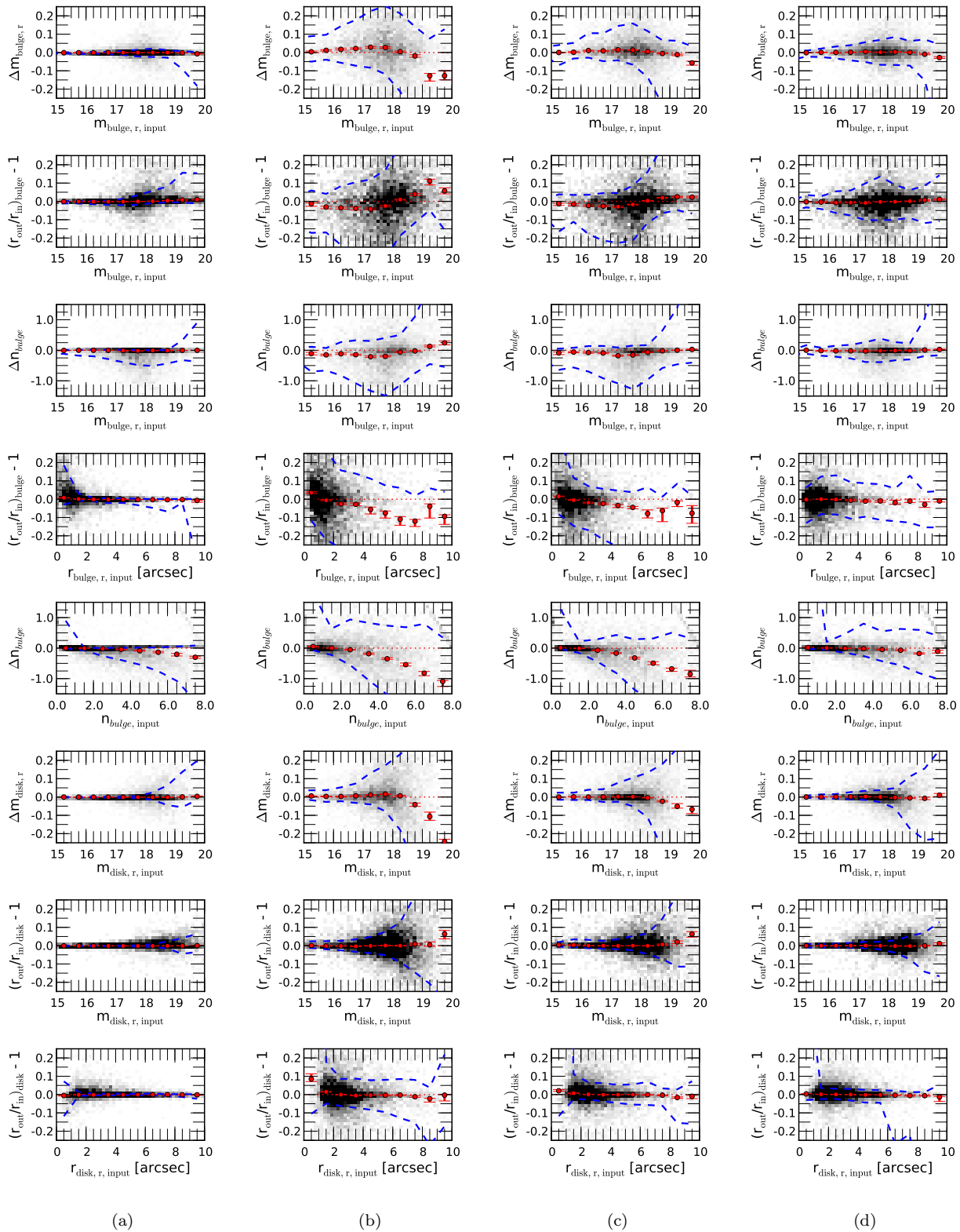


**Figure 10.** The simulated and recovered component parameters for a *SerExp* galaxy fit with a *SerExp* model in four cases: **a** the image prior to adding Poisson noise, **b** our fiducial case containing simulated sky, Poisson noise, PSF errors, and neighboring sources, **c** the fiducial case with S/N increased by a factor of 4, and **d** the fiducial case with resolution increased by a factor of 2. Over-plotted are the bias (red points) in the fitted values. All plots show the 68% (dashed line) scatter in blue. The density of points is plotted in gray-scale.

### 3.4 Varying the S/N and pixel size

In addition to the previous tests, we isolate the effects of the S/N and image resolution to quantify the contributions to the bias and scatter in our fits. Figures 6c, 7c, 8c, 9c, and 10c show the effect of increasing the S/N by a factor of 4 while holding all other parameters fixed. Similarly, Figures 6d, 7d, 8d, 9d, and 10d show the effect of increasing resolution by a factor of 2 while holding S/N constant. Corresponding decrements in these parameters were performed, although they are not presented in this paper.

Improving the resolution by a factor of two substantially improves the ability to recover the radius and Sérsic index with reduced bias. For instance, the Sérsic index bias is reduced to  $\approx 0.1$  at the larger values. Additionally, the bulge parameters of the **SerExp** fit improve substantially with improved resolution. Corresponding changes in the S/N reduce the scatter, but by a small amount relative to the effect of the resolution change. In addition, changing the S/N does not remove the observed bias in Sérsic index or bulge size. This leads us to conclude that the limitations of the resolution of SDSS are the leading factor in causing systematic offsets in the halflight radius, Sérsic index, and other fitting parameters (including the bulges of the **SerExp** fits). While increasing the S/N will reduce the scatter in the fits, increased resolution is necessary to properly recover unbiased values.

Lackner & Gunn (2012) also examined the effects of changing S/N and resolution on SDSS galaxies (see Figures 5-11 of their paper). The authors found that decreased resolution and S/N increases the relative error in the Sérsic index and radius. They recommended that **Ser** galaxies (and the bulge and disk sub-components of two-component galaxies) have radii,  $R_{hl} \gtrsim 0.5 \times \text{FWHM}$ . This cut removes  $\approx 1\%$  of the **Ser** mocks and  $\approx 22\%$  of the **SerExp** mocks from our simulated samples with a preference toward galaxies above  $z = 0.05$ .

While this condition is sufficient to keep the relative error in the halflight radius and Sérsic index comparable to the error in the magnitude, we find that this condition fails to remove the bias in our galaxy samples. Figure 6b shows that the underestimate of Sérsic index occurs at larger values. These galaxies tend to exhibit radii larger than the PSF. Given that the average FWHM of PSFs in our sample is  $\approx 1.3''$ , if we apply the suggested cut in radius, we are unable to remove the bias in Sérsic index. Clearly, reliable measurements are dependent on both the Sérsic index of the object and its radius relative to the resolution. Both parameters must be accounted for when deciding on an appropriate resolution cut.

If we extend the Lackner & Gunn (2012) recommendation to include a Sérsic index dependent term, this is sufficient to provide for recovery of Sérsic index  $> 4$  with bias  $\approx 0.1$  or  $\approx 1\%$ . Galaxies should have circularized halflight radii  $R_{hl} \gtrsim 0.5 * \text{FWHM} \times n$ . This removes nearly 75% of the sample. While such large cuts are sufficient to remove the bias in radius and Sérsic index for the **Ser** fits, the data are certainly biased relative to our original catalog after the cuts. Rather than remove these galaxies, we correct for the bias following a simple statistical argument presented in Section 4.

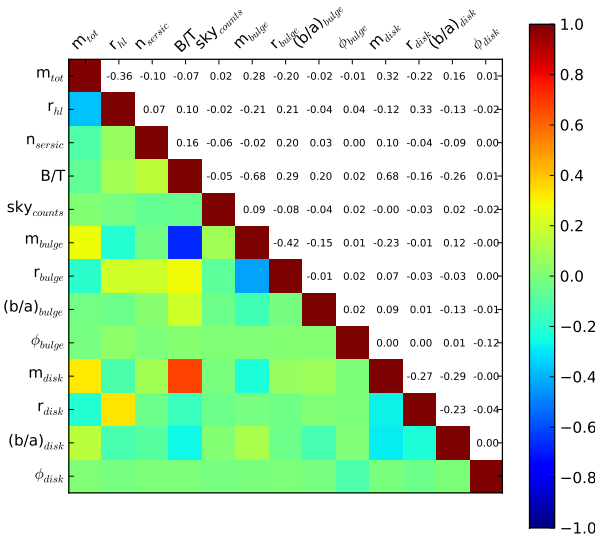


**Figure 11.** The correlation matrix for a mock **SerExp** galaxy fit with a **SerExp** model.

gesting that we have properly modeled the sky background and neighboring sources common to an SDSS spectroscopic galaxy.

Dense environments provide an additional test for our pipeline. To select fpC images that contain dense environments, we use the GMBCG catalog (Hao et al. 2011). We match brightest cluster galaxies (BCGs) with galaxies in our original catalog to select fpC images with cluster members including the BCG. Our mock galaxies are then inserted into the image which is run through the pipeline. In our previous simulations, intracluster light and gradients in the sky were not modeled. These tests allow us to see what the effects may be. Once again, the errors remain unchanged, showing that no environmental correction is necessary when using the fits from the pipeline.

Placing mock galaxies near cluster members allows us to test for systematic effects in crowded fields. However, further examination of BCG galaxies is necessary before we are able to properly model them for this purpose. For example, the curvature at the bright end observed in the size-luminosity relation of early-type galaxies (see Bernardi et al. 2013) appears to be due to an increasing incidence of BCGs, which define steeper relations than the bulk of the early-type population (e.g., Bernardi et al. 2007, 2013). However, the curvature could also be due to intracluster light (e.g., Bernardi 2009). Our ability to test the systematic effects associated with BCGs using the method outlined above is severely limited due to the existence of a BCG at the location we would prefer to place our test galaxy (i.e., the center of the cluster). Therefore, the stability of recovered fit parameters with respect to environment cannot be assumed to extend to BCGs based on the tests presented here alone. Further tests for the largest, brightest galaxies are needed to explore this possibility. We have not presented these tests in this text.

### 3.5 Effect of cutout size

We select postage stamp cutouts for use in fitting. It is important to select a cutout size that does not significantly bias the fits produced by PyMorph. The most important consideration is to provide enough sky pixels to allow the PyMorph program to properly determine the sky level in the images. Reducing cutout size may cause overestimation of background and corresponding errors in the other fit parameters. However, we use the PyMorph pipeline and GALFIT to fit a constant background to the galaxy image. Since a larger image could make sky gradients more significant, this could bias the fits when a larger cutout is used. We seek to minimize error when estimating the sky level without introducing a gradient term and further complicating the fitting process.

To test for optimal cutout size, we fit mocks with cutout sizes between 10 and 25 Petrosian half-light radii. We plot the average difference between simulated and measured fit parameters below. In Figure 12 we present the error and  $1\text{-}\sigma$  scatter in the error on the total magnitude, half-light radius and sky (showing SExtractor sky in blue and our estimates in red) as a function of cutout size. Smaller sizes clearly bias sky estimates made by SExtractor, but only minor improvement in the scatter of any parameters is achieved by using cutout sizes above 20 half-light radii. Since we use SExtractor sky as a starting point for our fitting, we choose a size of 20 half-light radii for our images. The sky estimates of SExtractor improve substantially. However, GALFIT sky estimation is stable over these sizes. Because GALFIT sky estimation is largely independent of the initial starting SExtractor value (which we would expect if we are truly finding the best fit to the galaxy), it is likely the case that cutout sizes smaller than even 10 half-light radii could be used for analysis.

Additional plots of other parameters are omitted in this section. The other fitted parameters show little or no sensitivity to cutout size in the range of cutout sizes used. However, as previously discussed, the bias and scatter may not be equally affected across all model parameters. The effects may be concentrated in a small part of the parameter space.

### 3.6 The effect of incorrect sky estimation

Estimation of the sky in the vicinity of the target galaxy has a high level of uncertainty. Indeed, accurate sky determination is likely not even a solvable problem as discussed briefly in Blanton et al. (2011). To determine the bias introduced by our sky estimation, we have tested our fitting pipeline in cases of both underestimation and overestimation of the sky. We fix the sky at the simulated sky level, as well as at simulated sky level  $\pm 0.5\%$  and  $\pm 1.0\%$ . These ranges were chosen to represent the range of differences between our sky estimations and those provided in the CASJOBS database for the SDSS spectroscopic sample.

Figure 13 shows a comparison of sky estimates using PyMorph to those provided from the SDSS photometric data pipeline. This comparison is performed on data from the catalog presented in M2013. The Figure shows the normalized distribution of differences in sky estimation in bins of 0.1%. A negative difference indicates that the sky measured by PyMorph is lower than that reported by SDSS. The vertical red solid line indicates the median of the distribution.

The red dashed, dot-dashed, and dotted lines indicate the 68-95-99% ranges of the data, respectively. The 95% range of sky values is approximately between  $\pm 1\%$  difference. For the test, we adopt this range as the range to test for sky variation.

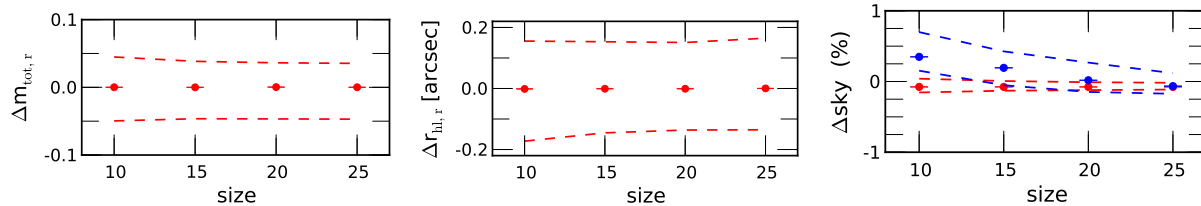
The results of incorrectly estimating the sky are shown in Figures 14 and 15. In red, we show the results of fitting galaxies using the standard PyMorph pipeline, treating sky level as a free parameter in the fit. PyMorph systematically underestimates the sky at the 0.1% level. However, the scatter is very tight as indicated by the vertical dashed red lines. In black we have plotted the fitting results at fixed sky levels of the correct value and  $\pm 0.5\%$  and  $\pm 1.0\%$ . Errors approaching 0.5% clearly introduce a large bias in the fits. The 0.5% level is an important level because it is the approximate level of overestimation shown in the preceding section (Section 3.5) found by SExtractor.

Note the asymmetry of the effects of incorrect sky estimation on fitting parameters. In particular, an underestimate of sky is much more detrimental to the fit than the corresponding overestimate. The reason for this asymmetry is due to changes in the perceived ‘‘flatness’’ of the profile at large radii. When the sky is overestimated, the galaxy profile tends to 0 flux too early. This causes a decrease in the Sérsic index and a decrease in the radius. However, when the sky is underestimated, there will be an extended, approximately constant brightness profile at larger radii. The only way to model such a profile is for Sérsic index to diverge to larger values which produce flat, extended profiles at large radii.

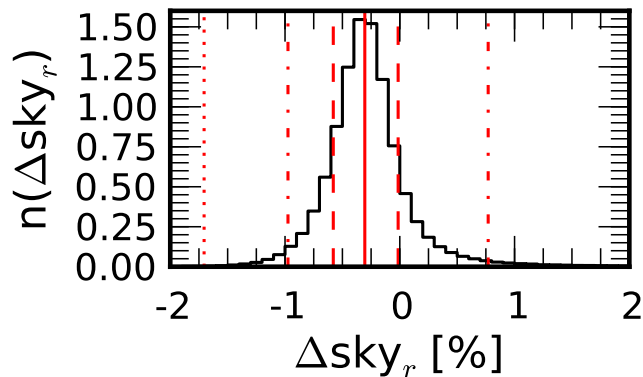
Guo et al. (2009) examined the effects of sky uncertainties in regards to the covariance between magnitude and both Sérsic index and half-light radius. They randomly sampled sky estimates from a distribution contained mostly within  $\pm 1\%$ . They found similar variation of Sérsic index (varying by 2 or more in some cases of underestimating the sky and varying by less than 1 in the case of overestimation). The asymmetry in bias due to incorrect sky estimation is apparent in Figure 5 of Guo et al. (2009), but not explicitly commented upon.

Figure 13 shows that PyMorph consistently estimates the sky  $\approx 0.25\%$  lower than that of the SDSS pipeline. Figures 12, 14, and 15 show that PyMorph has a systematic underestimate of the true sky at the  $\approx 0.1\%$  level. This bias is much smaller than the bias associated with using the SExtractor sky estimate as shown in Figure 13 (especially for smaller cutout size), which suggests that the sky values in SDSS are slightly overestimated.

**SerExp** disk components are remarkably robust to the errors in sky estimation, while bulge parameters suffer greatly, especially when the sky is underestimated. Upon further examination of Figure 15, the bulge parameters of the model are more accurately estimated when the sky is treated as a free parameter in the fit rather than when the sky is fixed at the correct value. However, this improvement does not suggest that underestimate of the sky is the preferred fitting outcome. It merely reflects the fact that the systematic effects due to underestimation of the sky are opposite to the underlying biases in half-light radius and Sérsic index. If we were to apply the PyMorph pipeline to an image with higher S/N and increased resolution, we would prefer the correct estimate of the sky to prevent systematic overestimate of these parameters.



**Figure 12.** The mean difference of the total magnitude (left column), PSF-corrected half-light radius (center column), and sky estimation (right column) as a function of cutout size for **SerExp** mocks fitted with a **SerExp** model. Other simulated models behave similarly. For sky estimation, the sky measured by GALFIT is plotted in red. SExtractor sky measurements are plotted in blue for reference. One- $\sigma$  scatter in the fits is plotted as a dashed line. Improvement in scatter when fitting for cutout sizes above 20 Petrosian radii is limited, so we use a 20 half-light radii cutout size for all images. Fit parameters seem to have no sensitivity to cutout size in this range, suggesting that it may even be possible to use smaller cutouts.



**Figure 13.** The percent difference between the sky estimate of PyMorph for SDSS galaxies and the sky estimated by the SDSS photometric pipeline for those same galaxies. The normalized distribution of differences is shown in bins of 0.1%. A negative difference indicates that the sky measured by PyMorph is lower than that reported by SDSS. The vertical red solid line indicates the median of the distribution. The red dashed, dot-dashed, and dotted lines indicate the 68-95-99% ranges of the data, respectively. The 95% range of sky values is approximately between  $\pm 1\%$  difference, so we adopt this as the range used to test the effects of improper sky estimation.

## 4 DISCUSSION

In the preceding sections we have shown the covariance, bias, and scatter in our parameter estimation for the **Ser** and **SerExp** models. In reality, the effects above will combine to yield a total scatter, covariance, and bias that should approach those shown in 3.2. Our simulations give us an idea of the behavior of the PyMorph pipeline when fitting SDSS galaxies as presented in M2013.

The simulations show that the recovery of global fitting parameters (total magnitude and half-light radius) in the case of SDSS galaxies is remarkably robust, even in the case of the **SerExp** fits. Two-component fits present a more difficult test for the pipeline. Both the bulge and disk components exhibit increased scatter relative to the scatter of the global parameters. In addition, the bulge component exhibits a systematic underestimation of the radius, Sérsic index, and magnitude, particularly for bulges with larger radii or higher Sérsic index.

The galaxies fit in M2013 have a median size roughly equivalent to the average PSF of SDSS. For most galax-

ies, the resolution necessary to accurately resolve bulge substructure is not present. As shown in Section 3.4, the ability to recover small bulges is improved by a factor of 2 increase in resolution. Finer resolution in central regions of the galaxy is also necessary to fully recover larger Sérsic indexes without bias. Even with these systematics, the two-component fits are still necessary to recover unbiased global parameters and can provide insight into the structure of galaxies.

The use of two-component models is potentially ill-advised for many SDSS galaxies as the respective sub-components may be too small to be well-resolved. This is suggested by Simard et al. (2011) as well as Lackner & Gunn (2012) (if we use the suggested resolution cut based on the PSF FWHM). However, our data show that this recommendation should be conditional on the galaxy parameters of interest. While it may be true that bulge parameters of the **SerExp** fit become unreliable at small radii, we show that using only the **Ser** fit radius will bias a sample of SDSS galaxies containing both single and two-component profiles (see Figure 8b). However, there are no cases where the **SerExp** fit introduces bias. It is advisable to use the **SerExp** half-light radius and magnitude as the total magnitude of the galaxy when examining a sample such as this.

The F-test offers a potentially powerful way to distinguish when it is necessary to use a more complicated two-component model. The F-test can compare the  $\chi^2$  values among nested linear models with Gaussian errors (Lupton 1993). Although our models are not linear and our error distribution is not strictly Gaussian, we apply the F-test to our fits. Following Simard et al. (2011), we adopt an F-test probability of 0.32 as the cutoff indicating a more complicated model is required. When we find a low F-test probability,  $P_{correct} < 0.32$ , the more complicated model (i.e., going from a one-component to two-component fit, or allowing the Sérsic index of the bulge to vary) provides a better fit to the observed profile. In cases where a **Ser** fit is used rather than a **SerExp** fit, the improvement in fitting is large enough to justify using a model with more free parameters. The improved fit is not merely the result of using a more flexible model. A similar test was performed by Lackner & Gunn (2012) to select among a pure disk or disk+bulge model.

If the selection based on the F-test is correct, then the resulting measurements of total magnitude and half-light radius will be unbiased. Using the **SerExp** mocks fit with each of the **Ser** and **SerExp** models, we select the fitted model by performing the F-test comparing the **Ser** and **SerExp**

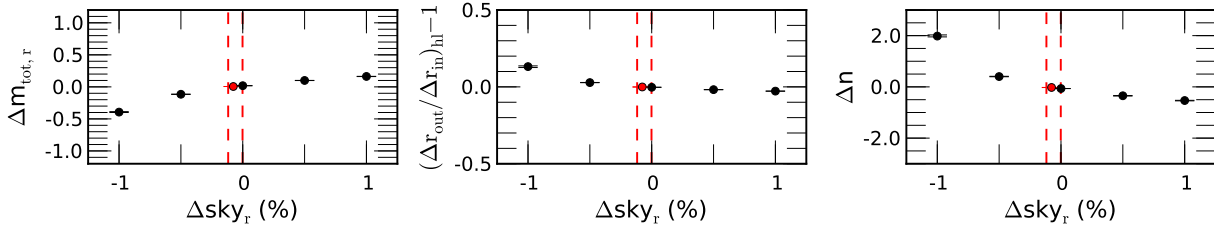


**Figure 14.** The simulated and recovered apparent magnitude (left), half-light radius (center), and Sérsic index (right) for a *Ser* galaxy fit with a *Ser* model. The residuals are plotted as a function of the sky level. Points plotted in black are from fits performed with fixed sky. The overplotted points in red are the result of fitting with sky level as a free parameter in the fit. The vertical dashed red lines mark the 68% scatter of the free sky determination. Our fits are slightly biased low, and this contributes to a small overall bias in fit parameters.

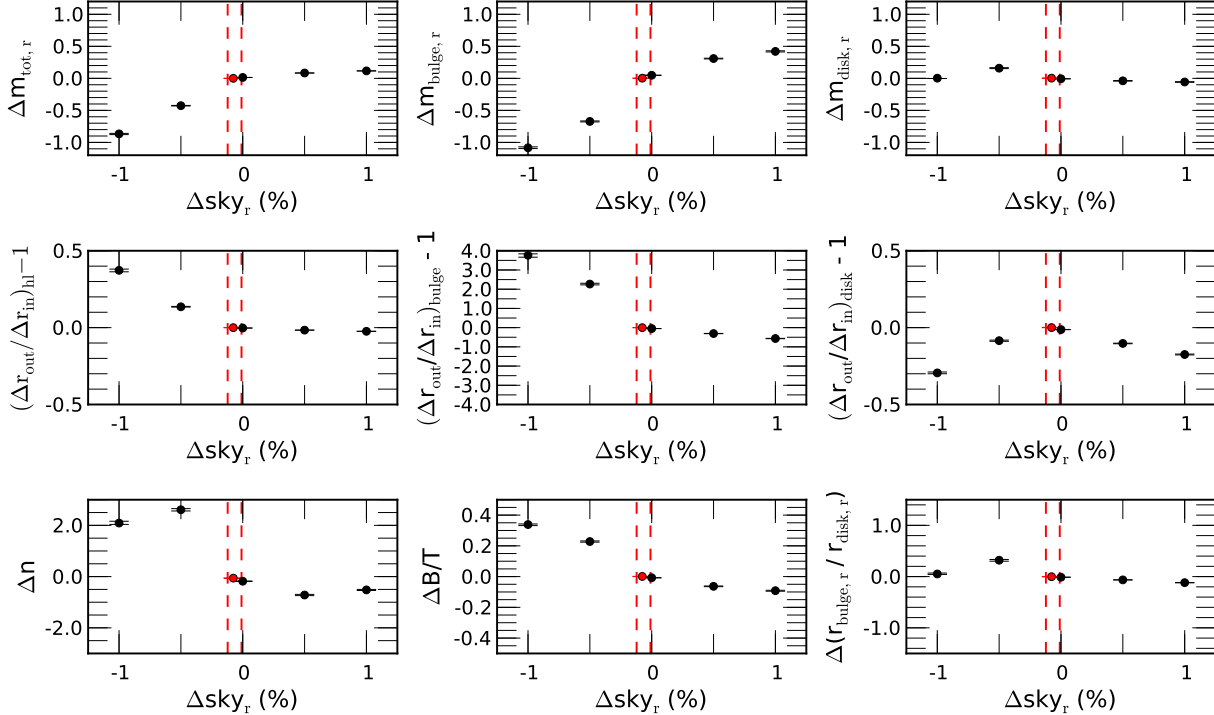


**Figure 15.** The simulated and recovered parameters of a simulated *SerExp* galaxy fit with a *SerExp* profile. The residuals are plotted as a function of the sky level. Points plotted in black are from fits performed with fixed sky. The overplotted points in red are the result of fitting with sky as a free parameter of the model. The vertical dashed red lines mark the 68% scatter of the GALFIT sky determination. Notice that disk parameters are relatively robust while bulge parameters suffer from incorrect sky estimation. Underestimates of sky level have a particularly strong effect on the bulge.

fits. The preferred fit (either *Ser* or *SerExp*) of the *SerExp* mocks is then used to assess the bias in the half-light radius and magnitude.

By examining the subset of *SerExp* mocks for which the F-test determines the *Ser* model to be the appropriate fit, we test the ability of the F-test to select galaxies that are correctly represented by *Ser* models. In Figure 16 we show the resulting distribution of total magnitude and half-light radius of this subset of *SerExp* mocks fit with *Ser* models. The bias originally observed in Figure 8b is not evident. However, the scatter in the recovered values are approximately twice as wide as in Figure 9b, indicating that while the fits are unbiased, some sensitivity is lost by using the simpler (and ultimately incorrect) model. The remaining *SerExp* mocks, for which the *SerExp* fit is determined

by F-test to be most appropriate, are also unbiased in total magnitude and half-light radius. From this test, we conclude that using the F-test to determine the most appropriate fitted model allows for unbiased measurement of the half-light radius and total magnitude.

Using the *Ser* mocks, the false positive rate (*Ser* mocks classified as needing a *SerExp* fit according to the F-test) for the F-test with a significance level of 0.32 is 5%, suggesting that there is a low level of contamination in a two-component sample selected using the F-test. Using *SerExp* mocks with  $0.2 < B/T < 0.8$  and  $n_{bulge} > 2$ , which we consider true two-component galaxies, the false negative rate (*SerExp* mocks classified as needing only a *Ser* fit according to the F-test) is 34%, missing a substantial fraction of the galaxies with two components. While selection using the F-

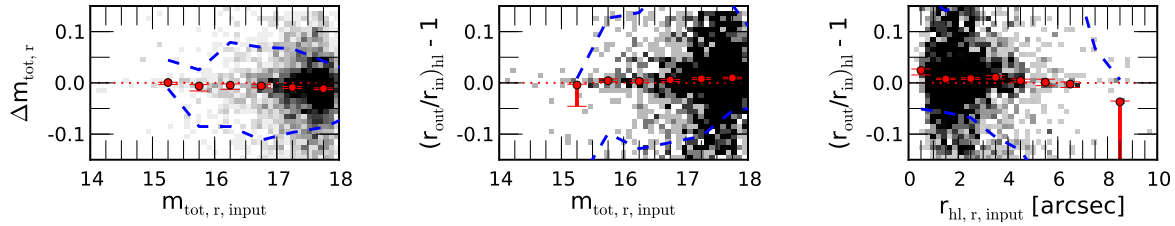


**Figure 16.** Total magnitude and halflight radius of **Ser** fits of **SerExp** mocks shown by F-test to be sufficiently well fit by **Ser** models. The fits are unbiased, but the scatter in the recovered values are approximately twice as wide in halflight radius and magnitude as compared to the **SerExp** fits in Figure 9b.

test is sufficient to remove the measured bias in global fitting parameters and is able to select a relatively pure sample of two-component galaxies, it does not select a complete sample of two-component galaxies. Clearly caution is necessary when using the F-test to select two-component galaxies from fitting routines. However, the F-test can indicate when the global parameters of a **Ser** model are likely unbiased regardless of the underlying galaxy type.

Following Simard et al. (2011), we can also select the fitted model based on a tiered approach, first performing the F-test on the **Ser** and **DevExp** fits. Galaxies for which the **DevExp** fit gives a statistically significant improvement are then tested again to determine whether the **SerExp** fit is preferable to the **DevExp** fit. The preferred fit (either **Ser**, **DevExp**, or **SerExp**) of the **SerExp** mocks is then used to assess the bias in the halflight radius and magnitude. We tested this approach and found that it did not significantly alter the results.

Many galaxies exhibit more complex structure than a single- or two-component structure. Even the case of a two-component model often oversimplifies galaxy structure. Bars, rings, central sources, clumpiness, or asymmetry cannot be effectively modeled in our simulations. Because of this, we can only determine a lower-bound on the uncertainty in our parameter estimates. However, correcting fits using this lower bound improves the fit of the observed galaxy.

We can apply a simple example of bias correction following the procedure outlined in Simard et al. (2002). Given the simulated and fitted values of the Sérsic index for the **Ser** model, we plot the bias as a function of the fitted value output by PyMorph. In this case, the output value represents the measured value in real data. The simulated value represents the true underlying value of the galaxy Sérsic index. We can determine an average bias and uncertainty in the bias, labeled as  $Bias$  and  $\Delta Bias$ , as a function of output Sérsic index. Additionally, we can measure the random error in the fits from the width of the bias distribution as a function of Sérsic index, labeled as  $\Delta Random$ . Then the corrected Sérsic index and uncertainty on the corrected index is

$$n_{corrected} = n_{fitted} - Bias(n_{fitted})$$

$$\Delta n = \sqrt{\Delta_{galfit}^2 + \Delta Bias^2 + \Delta Random^2} \quad (6)$$

Applying this correction allows us to correct bias as a function of both simulated and fitted Sérsic index for the sample

of galaxies used in M2013. We show the results of this process in Figure 17.

We are able to statistically correct for the bias in our sample in both the simulated and fitted bases for most values of the Sérsic index. However, there is an under-correction at high simulated Sérsic value. This effect appears to be due to the boundaries of the parameter space that PyMorph is allowed to search for the best fit model. By restricting PyMorph to values of  $n < 8$ , galaxies simulated with Sérsic index of 8 will be preferentially underestimated. However, the highest bins of fitted Sérsic index contain many more galaxies with over-estimated Sérsic index. Therefore the net correction will be negative and not appropriate for the highest bins. We could improve the error correction at higher bins by allowing GALFIT to explore larger values of the Sérsic index. However, this is beyond the scope of this paper.

Additional corrections may also be considered (i.e., divide in both magnitude and Sérsic index prior to computing the bias correction) depending on the specifics of a given study. For properties of the global population, the corrections measured in this paper are applicable to the sample presented in M2013.

Our tests were performed on r-band data from SDSS. The performance of the pipeline can change when observing in different bands. This change is primarily dependent on the change in the S/N and resolution between bands (due to the changing brightness of the sky, color of the galaxy, and size relative to the PSF) and on the different galactic structures to which neighboring SDSS filter bands are sensitive. In principle, these effects could be measured from the simulations presented in this paper by adjusting the S/N and background level. Additionally, one may have to adjust the size of the galaxies or redraw the sample to match the size distributions in the different band. In M2013, we fit the SDSS g, r, and i band data. It is unlikely that the images change drastically enough over the wavelength and redshift range observed to require additional testing in the i band. However, these simulations become an increasingly poor estimate of error in bluer bands where the photometry becomes more sensitive to star forming regions. These regions tend to be clumpier and, therefore, less well represented by a smooth profile. Therefore, g band fits may present more scatter than the r or i band data. These clumpy regions are difficult to model with the smooth models presented here. One could attempt a hybrid approach to generating simulated data whereby one isolates clumpiness in nearby galaxies and use this as a template to add clumpiness to

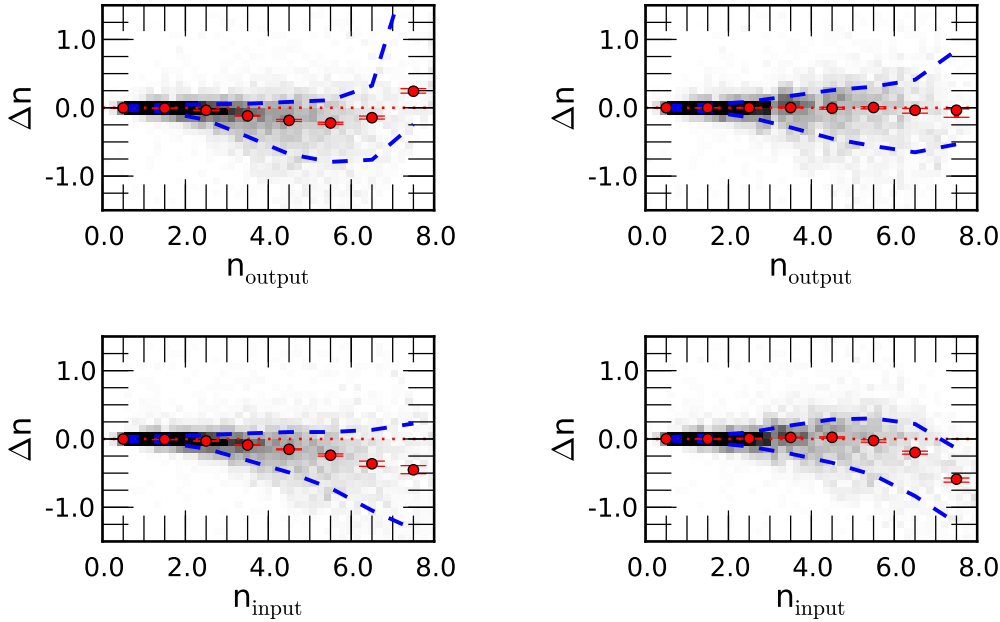


**Figure 17.** An example of the bias correction of the Sérsic index of the *Ser* model. The error in the Sérsic index ( $n_{output} - n_{input}$ ) versus output value is presented before (top left panel) and after (top right panel) correction. The same correction is shown in the bottom row versus the simulated value of the Sérsic index. We apply the correction in the  $n_{output}$  basis. This appropriately corrects the bias as a function of  $n_{input}$  except at high  $n$  where the correction fails. The reason for this failure is due to the boundaries of the allowed  $n$  parameter space. Galaxies in the highest bins of output Sérsic index are a combination of poorly fit, low Sérsic index galaxies that are artificially constrained to fall in the high bins, and correctly fit, high Sérsic index galaxies. The result of this mixture is a net negative correction on galaxies with high Sérsic index.

smaller SDSS galaxies. However, the details of this process are beyond the scope of this paper.

It is also potentially useful to use information about the r-band to inform the fits of neighboring bands. Indeed Simard et al. (2011) attempted this by requiring many parameters (i.e., Sérsic index, radius, ellipticity) of the fitting model to be identical across the g and r bands, essentially using the two bands as a form of coadded data to increase the S/N. This increase of S/N comes at the expense of dis-allowing variation in the matched parameters, which may or may not be an appropriate assumption (i.e., in a two-component fit, we might expect the bulge size to change across bands, which is dis-allowed). Additionally, Häußler et al. (2013) enforced simple polynomial relationships in parameters across bands, using the neighboring bands to further constrain the acceptable parameter space to be searched by the fitting algorithm. The most flexible method is to fit each band independently and examine the systematic effects of each band as necessary, making additional cross-band comparisons including color (for example, see Lackner & Gunn 2012). This is our preferred method for the data presented here and in M2013.

## 5 CONCLUSION

We presented the simulations used to test fitting of SDSS galaxies using PyMorph. Simulations of the *Ser* and *SerExp* models were presented and examined in many different cases. The simulations were generated using the results of

the fits presented in M2013. We showed that our simulations are recoverable in the case of no noise, which demonstrates that our simulations are correct. We then showed that we can recover the parameters in the case of a simulated background and noise representative of the average SDSS image (see Figures 6, 7, 8, 9, and 10).

Several individual effects on the fitting were examined. We showed that our choice of 20 half-light radii for cutout size does not significantly bias our fitting results (see Figure 12). In addition, we examined the effect of incorrect background estimation, which can significantly affect fitting results (Figure 14 and 15). Effects of increasing the S/N are somewhat limited for this sample. However, an increase in the resolution of the sample would greatly improve parameter measurements, removing many biases in the two-component fits and improving the estimation radius and Sérsic index for *Ser* galaxies as shown in Figures 6d and 10d.

We also examined the bias created when fitting incorrect models to galaxies. Fitting a two-component Sérsic + Exponential model to what is really just a single Sérsic results in a noisier recovery of the input parameters, but these are not biased (see Figure 7b); fitting a single Sérsic to what is truly a two-component system results in an overestimate of 0.05 magnitudes in total magnitude and 5% half-light radius for dim galaxies, increasing to 0.1 magnitudes and 10% for galaxies at the brighter end of the apparent magnitude distribution (see Figure 8b). These biases are used to correct the systematics of our fitted SDSS sample and suggest that magnitude and radius values of a *SerExp* fit are the least likely to be biased across many galaxy types. Therefore it

is advisable to use **SerExp** values when examining global parameters for galaxies.

These simulations can be analyzed together with the fits presented in M2013 to give a more detailed understanding of galaxy structure and formation as presented in Bernardi et al. (2013).

## ACKNOWLEDGMENTS

The authors would like to thank the anonymous referee for many useful comments that helped to greatly improve the paper. AM and VV would also like to thank Mike Jarvis and Joseph Clampitt for many helpful discussions.

This work was supported in part by NASA grant ADP/NNX09AD02G and NSF/0908242.

Funding for the SDSS and SDSS-II has been provided by the Alfred P. Sloan Foundation, the Participating Institutions, the National Science Foundation, the U.S. Department of Energy, the National Aeronautics and Space Administration, the Japanese Monbukagakusho, the Max Planck Society, and the Higher Education Funding Council for England. The SDSS Web Site is <http://www.sdss.org/>.

The SDSS is managed by the Astrophysical Research Consortium for the Participating Institutions. The Participating Institutions are the American Museum of Natural History, Astrophysical Institute Potsdam, University of Basel, University of Cambridge, Case Western Reserve University, University of Chicago, Drexel University, Fermilab, the Institute for Advanced Study, the Japan Participation Group, Johns Hopkins University, the Joint Institute for Nuclear Astrophysics, the Kavli Institute for Particle Astrophysics and Cosmology, the Korean Scientist Group, the Chinese Academy of Sciences (LAMOST), Los Alamos National Laboratory, the Max-Planck-Institute for Astronomy (MPIA), the Max-Planck-Institute for Astrophysics (MPA), New Mexico State University, Ohio State University, University of Pittsburgh, University of Portsmouth, Princeton University, the United States Naval Observatory, and the University of Washington.

## REFERENCES

- Abazajian K. N. et al., 2009, *ApJS*, 182, 543  
 Abraham R. G., Tanvir N. R., Santiago B. X., Ellis R. S., Glazebrook K., van den Bergh S., 1996, *MNRAS*, 279, L47  
 Bernardi M., 2009, *MNRAS*, 395, 1491  
 Bernardi M., Hyde J. B., Sheth R. K., Miller C. J., Nichol R. C., 2007, *AJ*, 133, 1741  
 Bernardi M., Meert A., Vikram V., Huertas-Company M., Mei S., Shankar F., Sheth R. K., 2013, *MNRAS* submitted,  
 Blanton M. R. et al., 2001, *AJ*, 121, 2358  
 Blanton M. R. et al., 2003, *ApJ*, 592, 819  
 Blanton M. R., Kazin E., Muna D., Weaver B. A., Price-Whelan A., 2011, *AJ*, 142, 31  
 Blanton M. R. et al., 2005, *AJ*, 129, 2562  
 Caon N., Capaccioli M., D’Onofrio M., 1993, *MNRAS*, 265, 1013  
 de Vaucouleurs G., 1948, *Annales d’Astrophysique*, 11, 247  
 Freeman K. C., 1970, *ApJ*, 160, 811  
 Graham A. W., Driver S. P., 2005, *PASA*, 22, 118  
 Guo Y. et al., 2009, *MNRAS*, 398, 1129  
 Hao J. et al., 2011, in *Bulletin of the American Astronomical Society*, Vol. 43, American Astronomical Society Meeting Abstracts #217, p. 213.06  
 Häußler B. et al., 2013, *MNRAS*, 430, 330  
 Häußler B. et al., 2007, *ApJS*, 172, 615  
 Huertas-Company M., Shankar F., Mei S., Bernardi M., Aguerri J. A. L., Meert A., Vikram V., 2012, *ApJ* submitted,  
 Kelvin L. S. et al., 2012, *MNRAS*, 421, 1007  
 Kent S. M., 1985, *ApJS*, 59, 115  
 Lackner C. N., Gunn J. E., 2012, *MNRAS*, 421, 2277  
 Lupton R., 1993, *Statistics in theory and practice*  
 Lupton R., Gunn J. E., Ivezić Z., Knapp G. R., Kent S., Yasuda N., 2001, in *Astronomical Society of the Pacific Conference Series*, Vol. 238, *Astronomical Data Analysis Software and Systems X*, Harnden Jr. F. R., Primini F. A., Payne H. E., eds., p. 269  
 Meert A., Vikram V., Bernardi M., 2013, *In Prep*,  
 Peng C. Y., Ho L. C., Impey C. D., Rix H.-W., 2002, *AJ*, 124, 266  
 Petrosian V., 1976, *ApJ*, 209, L1  
 Press W. H., Teukolsky S. A., Vetterling W. T., Flannery B. P., 1992, *Numerical recipes in C. The art of scientific computing*  
 Sérsic J. L., 1963, *Boletín de la Asociación Argentina de Astronomía La Plata Argentina*, 6, 99  
 Shankar F., Marulli F., Bernardi M., Mei S., Meert A., Vikram V., 2013, *MNRAS*, 428, 109  
 Shen S., Mo H. J., White S. D. M., Blanton M. R., Kauffmann G., Voges W., Brinkmann J., Csabai I., 2003, *MNRAS*, 343, 978  
 Simard L., Mendel J. T., Patton D. R., Ellison S. L., McConnell A. W., 2011, *ApJS*, 196, 11  
 Simard L. et al., 2002, *ApJS*, 142, 1  
 Strauss M. A. et al., 2002, *AJ*, 124, 1810  
 Vikram V., Wadadekar Y., Kembhavi A. K., Vijayagovindan G. V., 2010, *MNRAS*, 409, 1379